Waves and structure interaction using multi-domain couplings for Navier-Stokes solvers in OpenFOAM®. Part II: validation and application to complex cases

Benedetto Di Paolo[a,*], Javier L. Lara[a], Gabriel Barajas[a], Íñigo J. Losada[a]

[a]*IHCantabria - Instituto de Hidráulica Ambiental de la Universidad de Cantabria*
C/Isabel Torres nº 15, Parque Científico y Tecnológico de Cantabria, 39011 Santander, Spain.

Abstract

In this work, we present several applications of the 2D-3D multi-domain couplings for Navier-Stokes models developed and validated in its companion (Di Paolo et al., submitted). The methodology is used to carry out some relevant simulations which include long regular and irregular waves, solitary wave propagation on a shallow foreshore, focused wave group transformation on a planar beach, wave impact on a cylinder and finally, the numerical twin of a complex laboratory experiment to analyse the performance of a perforated breakwater under wave action.
Results agree well with the full 3D simulations and laboratory experiments and demonstrate the feasibility of using the 2D-3D coupled methodologies presented in Part I to successfully replace full 3D modelling. For all the cases considered, the application of coupled methodologies have resulted in a drastic reducing of the computational time without decreasing the accuracy of the full solution.

Keywords: Coupled models, Navier-Stokes, One-way, Two-way, OpenFOAM, wave-structure interaction

1 Introduction

Numerical models have become a well-established tool for wave-structure interaction studies in coastal and offshore environments as they are perfect complement to physical experiments. Numerical models are normally used for wave generation, propagation, transformation and interaction with structures with an increasing level of accuracy from far to near field. It is well recognized that simplified models (e.g. Non-linear shallow water and Boussinesq solvers) can deal with wave generation, propagation and transformation till the toe of structures (e.g. Zijlema et al. (2011), Brocchini (2013), Kirby (2016)).

However, a proper analysis of wave-structure interaction generally requires a full 3D model in order to account for fluid viscosity and directly solve breaking and other dissipation processes. Although it is well known that the full 3D CFD models accurately simulate wave interaction with fixed and movable structures (e.g. Higuera et al. (2013), Gotoh and Khayyer (2018), Chen et al. (2019)), the application to large domains is still unfeasible (Vandebeek et al. (2018)).

*corresponding author
Email addresses: benedetto.dipaolo@unican.es (Benedetto Di Paolo), jav.lopez@unican.es (Javier L. Lara), gabriel.barajas@unican.es (Gabriel Barajas), inigo.losada@unican.es (Íñigo J. Losada)

For this reason, coupled methodologies in which different numerical models are working together have been rapidly increasing in the last few years as described in Part I (e.g. Kim et al. (2010), Sriram et al. (2014), Verbrugghe et al. (2018), Mintgen and Manhart (2018), Sitanggang and Lynett (2010), Martínez-Ferrer et al. (2016)).

To date, several coupled simulations have been applied to study the response of structures. Hildebrandt et al. (2013) simulated wave loads on a tripod structure, considering strong 3D flow in the near field and neglecting wave reflection. El Safti et al. (2014) also studied a similar topic, considering rogue wave impacts on a cylinder. Sitanggang and Lynett (2010) reproduced a large-scale tsunami overtopping on a breakwater but the simulations were purely 2D. Pure 2D simulations were also carried out by Verbrugghe et al. (2018) for an oscillating water column (OWC) and for a floating box under waves. The main drawback was that 3D effects around the structures were not taken into account. Martínez-Ferrer et al. (2018) applied the implementations presented in Martínez-Ferrer et al. (2016) to study the interaction of two-phase fluid flows with elastic structures. Mintgen and Manhart (2018) developed coupled simulations to estimate forces and drag coefficient for flood wave impacts on an obstacle. They also validated the 2D-3D (shallow water - RANS) coupling when the shallow water hypothesis was violated, thus extending the range of application of the code.

In general in wave and structure interaction the three-dimensional flows are dominant in the near field close to the structures while they lose importance in the far field. Particularly, this can be accepted when waves impact normally on the structures, which usually occur for wave interaction with breakwaters. When the geometry of the breakwater does not change in the spanwise direction a 2D model is usually applied (e.g. Losada et al. (2008), Jacobsen et al. (2018), Di Lauro et al. (2019), Lara et al. (2019)) otherwise a full 3D model is essential (e.g. Dentale et al. (2018), Tsai et al. (2018), Wang et al. (2019)). Wang et al. (2019) investigated the performance of a perforated breakwater comparing physical experiments with 2D and 3D numerical simulations. They showed that the 2D numerical models (CFD) are inadequate to estimate the wave reflection coefficient, pressure and velocity fields, while the 3D numerical results successfully matched the laboratory data but in exchange for an extremely high computational time.

With the aim of reducing the computational time without decreasing the accuracy of a full 3D model, multi-domain 2D-3D couplings for Navier-Stokes models were implemented in Part I (Di Paolo et al., submitted). An extensive analysis of the couplings methods to transfer information between 2D and 3D domains was conducted showing a good correlations with full solutions (3D).

In this paper, the new methods are implemented in the simulation of more practical case studies. Long time series of regular and irregular waves and a solitary wave propagating on a shallow foreshore are simulated first. The evolution and breaking of regular and focused waves on a planar beach are modelled next. A focused wave group impacting on a cylinder is also studied. The results of the coupled simulations are compared with full 3D solutions. Finally, the numerical twin of the laboratory experiment of a perforated breakwater (Wang et al. (2019)) is reproduced and validated.

2 Application of the 2D-3D coupling methodology

The main aim of this paper is to present practical applications of the coupling methods implemented and validated within Part I (Di Paolo et al., submitted). Exploring the ability of the methods to reproduce complex flows characterised by three-dimensionality (e.g. breaking waves, wave structure interaction) is required in order to test their potential application to real studies. The case studies selected are presented next, in order of increasing complexity.

2.1 Long duration wave series

With the aim of studying long duration of wave time series the influence of the coupling methodology in passing long series of information through the 2D and 3D regions needs to be assessed.

A time series of regular waves has been generated first using the coupling setups in Figure 1 in one-way (panel a) and two-way (panel b) modes and the results are compared with the full 3D simulation.

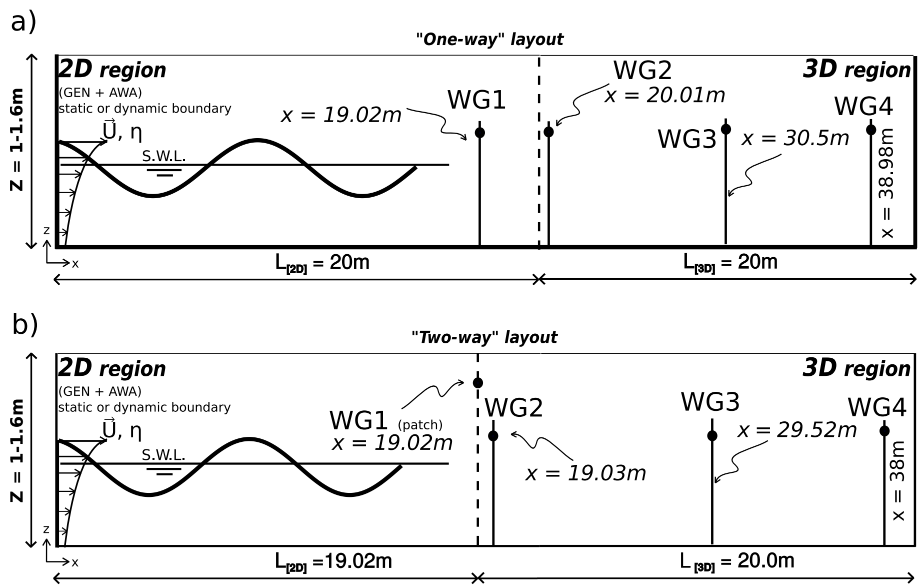

Figure 1: Numerical domain used for the one-way (panel a) and two-way (panel b) simulations.

The numerical setup for the one-way and two-way methodologies are the same as defined in the validations within Part I (Figure 7). A 20m long, 0.04m wide (1 cell) and 1.6m high (1.0m for irregular wave cases) numerical domain (x-z plane) has been defined for the 2D region, while a 20m long, 0.4m wide (10 cells) and 1.6m high (1.0m for irregular wave cases) domain has been built for the 3D region. An aspect ratio (Δ_x/Δ_z) of 1.0 has been considered to better reproduce the curvature of the free surface in time series of irregular waves. Such aspect ratio is also suggested in literature (Larsen et al. (2019)). Δ_x is 0.01m, Δ_y is 0.04m, Δ_z is 0.01m and the total span-wise length is 0.4m. In all cases of long duration wave series the time step has been adjusted such that a maximum Courant number of ($C_o = |u_i|\Delta_t/\Delta_{x_i} = 0.1$) has been kept at all time steps. The simulations have been run in laminar mode. Active wave absorption has been defined at the outlet of the 3D region. All the two-way simulations carried out in Part II made use of the stabilisation on both 2D and 3D interfaces (see Di Paolo et al., Part I submitted).

The wave parameters are indicated in Table 1. H_{mo} is the spectral significant wave height and T_p stands for peak period.

Case	h**(m)**	H**(m)**	T**(s)**	H_{mo}**(m)**	T_p**(s)**	γ
RW	1.1	0.12	2.5	-	-	-
IW1	0.6	-	-	0.05	2.0	3.3
IW2	0.4	-	-	0.05	4.0	3.3

Table 1: Wave parameters for long time series. A JONSWAP spectrum is used for the irregular wave cases.

Figure 2 shows a comparison of the free surface elevation (ζ) for the one-way , two-way and 3D simulations, considering time windows in the range 30s<t<170s. For the one-way simulations, results are shown at four positions of the sampling sensors as considered in Part I. The four positions are x_1 = 19.02m (WG2 in Figure 1), x_2 = 19.8m, x_3 = 19.9m and x_4 = 19.985m.

Regarding the one-way results it can be observed that by changing the position of the sampling sensor, the free surface elevation is not strongly affected. Very small deviations are observed among signals throughout the long simulation (panels from a to d of Figure 2). Wave heights do not vary significantly in time. Even when placing the sensor close to the absorbing boundary, the results are satisfactory although a small increase of free surface elevation is observed. Panel a) shows that very small discrepancies are observed between the 3D results and the one-way simulations. It can also be observed that when placing the sampling sensor far from the coupling boundary (x_1), the free surface elevation is correctly predicted throughout the simulation time (panels from a to d). The discrepancies slightly increase in time (panel b, c and d) and in particular for position x_4, i.e. 1.5 cells far from the outlet of the 2D domain (worst scenario). The most evident discrepancy is shown in panel c, where a zoom at the wave crest (114.6s<t<115.2s) is shown. The maximum error is however below 7% in this case. By observing the two-way results it can be seen that the performance are comparable with the 3D simulation. Wave heights are correctly predicted and no significant phase lag are shown. On average, both coupled models (one-way and two-way) preserve the shape of the wave.

Next, two irregular sea states (1 hour) have been simulated using both coupled models (one-way and two-way) and 3D solutions. Here, comparisons are provided in terms of free surface elevation and power spectral density (PSD) at WG2, WG3 and WG4. The significant (spectral) wave height (H_{mo}) is also calculated comparing the results of the coupled (one-way and two-way) and the 3D simulations.

Figure 3 displays comparisons between the energy spectra of the free surface elevation measured at WG2, WG3 and WG4. It can be clearly observed that both coupled models give results close to the full solution in terms of wave spectra (panels a, b and c). The one-way model shows a small over-prediction of the peak spectra at WG2 (panel a) while the two-way model displays

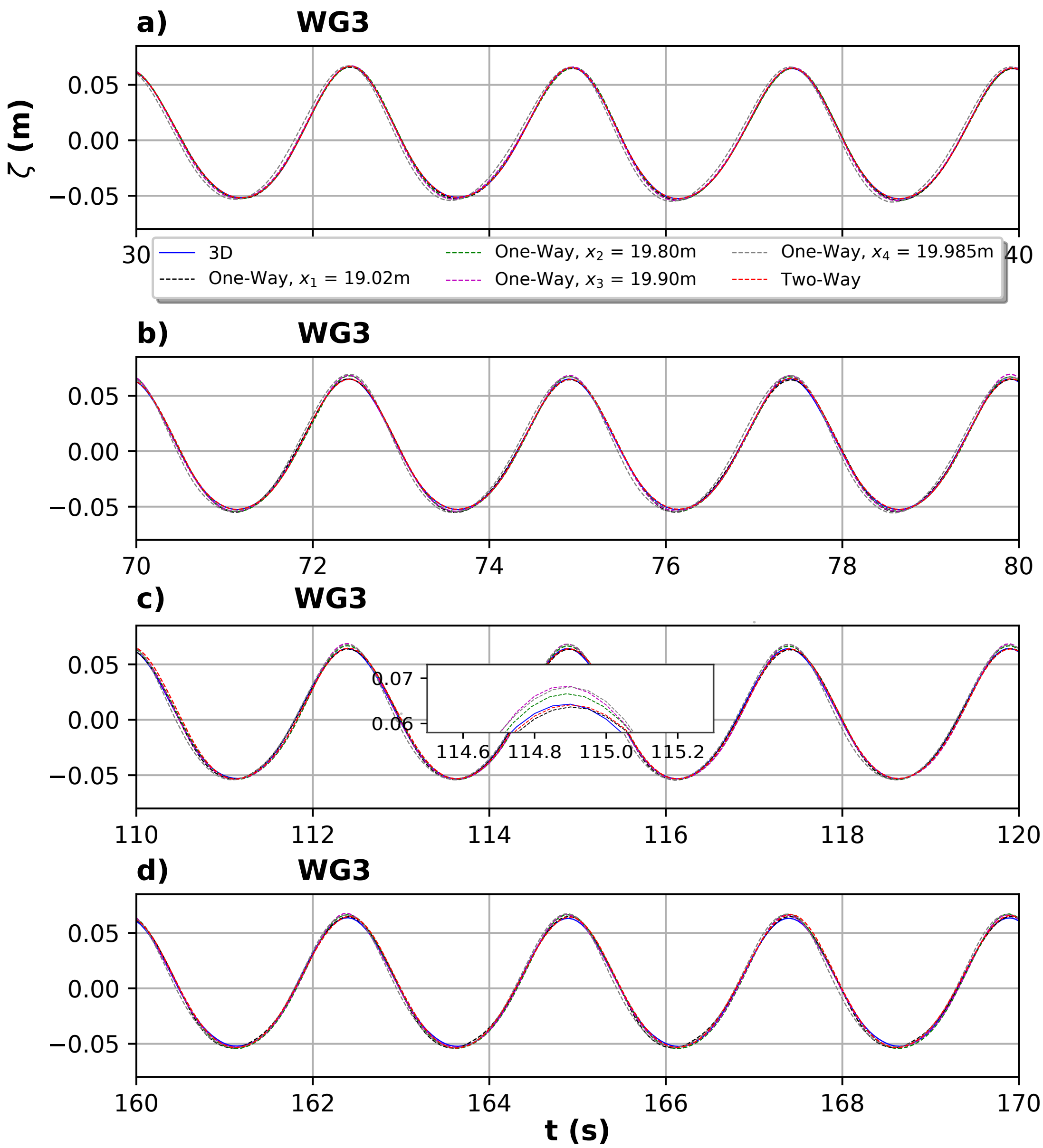

Figure 2: Case RW in Table 1. Numerical results of one-way, two-way and 3D simulations at WG3. H = 0.12m, T = 2.5s, h = 1.1m.

a better correlation with the full solution. The one-way model seems to slightly over-predict the high-frequency components but again the discrepancy with the 3D results is very small (panel a). In the far-field, at WG3 and WG4, both coupled models perform well and the results match the 3D solution (panels b and c). The significant wave height appears to be correctly estimated by both coupled models throughout the numerical domain (Table 2). The only discrepancy observed is for the significant wave height obtained with the one-way model at WG2 (0.049m) which slightly dif-

	IW1 - H_{mo}(m)			IW2 - H_{mo}(m)		
	oneWay	**twoWay**	**3D**	**oneWay**	**twoWay**	**3D**
WG2	0.049	0.048	0.048	0.046	0.046	0.046
WG3	0.048	0.048	0.048	0.046	0.046	0.046
WG4	0.048	0.048	0.048	0.046	0.046	0.046

Table 2: Spectral significant wave heights for the coupled and 3D simulations at WG2, WG3 and WG4. Results for IW1 and IW2 (Table 1) are shown.

	IW1		IW2	
	Cr$_{2d}$(%)	**Cr**$_{3d}$(%)	**Cr**$_{2d}$(%)	**Cr**$_{3d}$(%)
oneWay	0.12	0.12	0.14	0.13
twoWay	0.11	0.12	0.14	0.13
3D	0.11	0.12	0.14	0.13

Table 3: Wave reflection coefficients in each region (i.e. 2D and 3D).

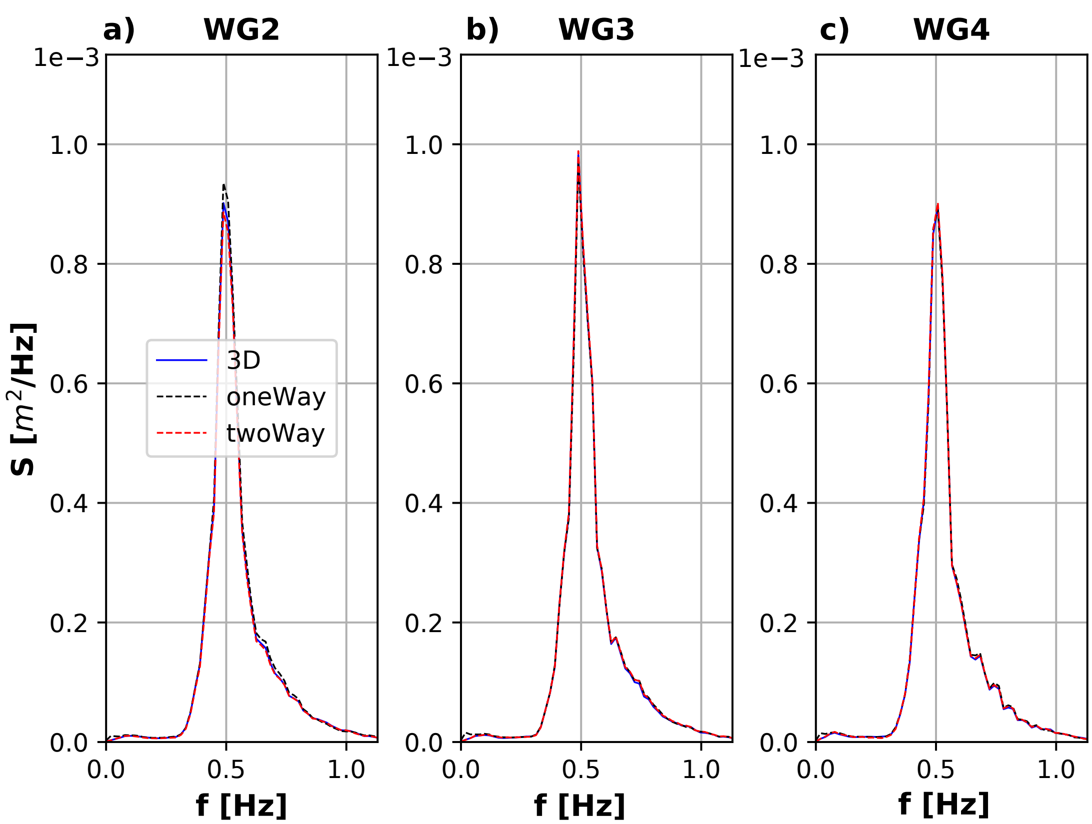

Figure 3: Case IW1 in Table 1. Power spectral density (PSD) obtained from one-way, two-way and 3D simulations. Comparison at WG2, WG3 and WG4.

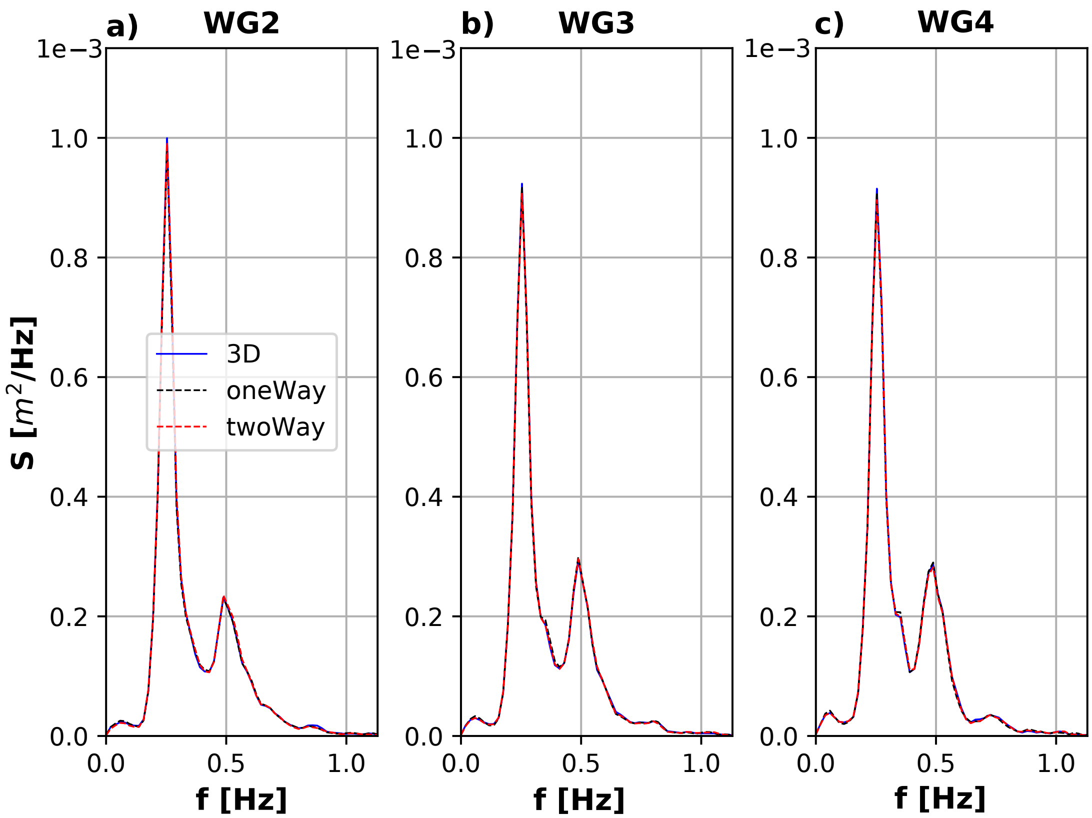

Figure 4: Case IW2 in Table 1. Power spectral density (PSD) obtained from one-way, two-way and 3D simulations. Comparison at WG2, WG3 and WG4.

fers from the 3D calculation (0.048m). The reflection coefficient has also been estimated. The wave gauge arrays have been placed inside the 2D and 3D regions of the coupled models. For the 3D models the wave gauge arrays have been defined in the same positions as for the coupled models, thus allowing to calculate the wave reflection coefficients analogous to the 2D and 3D regions of the coupled models. The wave reflection coefficient calculated inside the 2D and 3D domains are defined as Cr_{2d} and Cr_{3d}, respectively (Table 3). It can be observed that both coupled and 3D models lead to the same values of the wave reflection coefficient (Table 3). The main result is that the coupling methodologies do not increase or decrease wave reflection for the cases considered and the wave reflection coefficient remain almost constant throughout the numerical domain.

Figure 4 shows the results for the irregular wave case IW2. Here, a very good correlation is observed for both coupled models and 3D solution at WG2, WG3 and WG4 (panels a, b and c). Again, the significant wave height appears to be correctly estimated by both coupled models throughout the numerical domain (Table 2). H_{mo} remains constant throughout the spatial domains for all models. Also, the wave reflection coefficient is identically obtained by using the one-way, two-way and 3D simulations (Table 3).

In conclusion, good results can be obtained with the coupled models when considering long time series of regular and irregular waves. For regular waves both coupled models perform well in terms of free surface elevation showing acceptable deviations with the 3D solutions. The two-way model gives results very close to the 3D simulations, while the one-way solution shows small deviations, particularly when the sampling sensor is closer to the coupled interfaces. However, the error was always below 7%. Regarding the irregular waves, the coupled models give results close to the full solution, in terms of wave spectra and significant wave height for both cases considered. Also, the coupled models lead to the same wave reflection coefficients obtained with the 3D solutions, demonstrating that the couplings do not increase or decrease significantly the wave reflection.

2.2 Coupling in shallow foreshores

One way to decrease the computational cost is by pushing the coupling interfaces close to the structures as much as possible. For nearshore hydrodynamics this may require establishing the coupling zone in shallow foreshores. So it is key to verify that the methodologies introduced (one-way and two-way) are capable of correctly transferring information over a shallow foreshore.

A numerical 2D-3D domain is defined, as shown in Figure 5, to simulate the transformation of a solitary wave on a shallow foreshore. The dimensions of the domain are as follows: L[2D]$_{one-way}$=34.125m, L[3D]$_{one-way}$=11.125m, L[2D]$_{two-way}$=34.02m, L[3D]$_{two-way}$=11.125m.

Mesh discretization (both 2D-3D regions): Δ_x = 0.02m, Δ_y = 0.02m, Δ_z = 0.02m (12 cells per wave height). The maximum Co has been set to 0.1. The stabilised $k-\omega$ turbulence model has been used. Target wave conditions at the wave-maker position are: H=0.25m, h=1.18m. WG1 and WG2 are placed at x=35.13m and x=37.605m, respectively, and are used to measure velocity and dynamic pressure profiles.

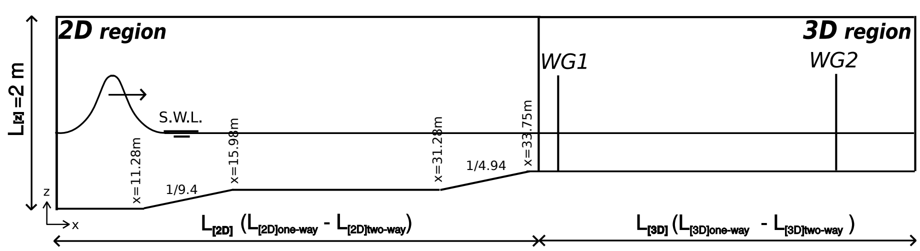

Figure 5: Numerical domain. Solitary wave propagating on a shallow foreshore.

Figure 6 shows the free surface elevation, velocity and dynamic pressure profiles of the one-way, two-way and 3D simulations, displayed with dashed black, dashed red, and blue lines, respectively. The free surface is compared at WG1 and WG2 (see Figure 5). From panel a), it can be observed that results are well correlated throughout the simulation, although the one-way solution provides a slightly higher wave crest than the two-way simulation ($t \approx 12s$). Furthermore, results for the coupled models are consistent with the ones for the full model. The development of the soliton is well captured by both models ($13s < t < 16s$). In panel b it can be observed that the free surface transformation along the three-dimensional domain ($x = 37.98m$) matches well the full solution for both one-way and two-way couplings, although in this case the two-way model appears to slightly under-predict the wave peak.

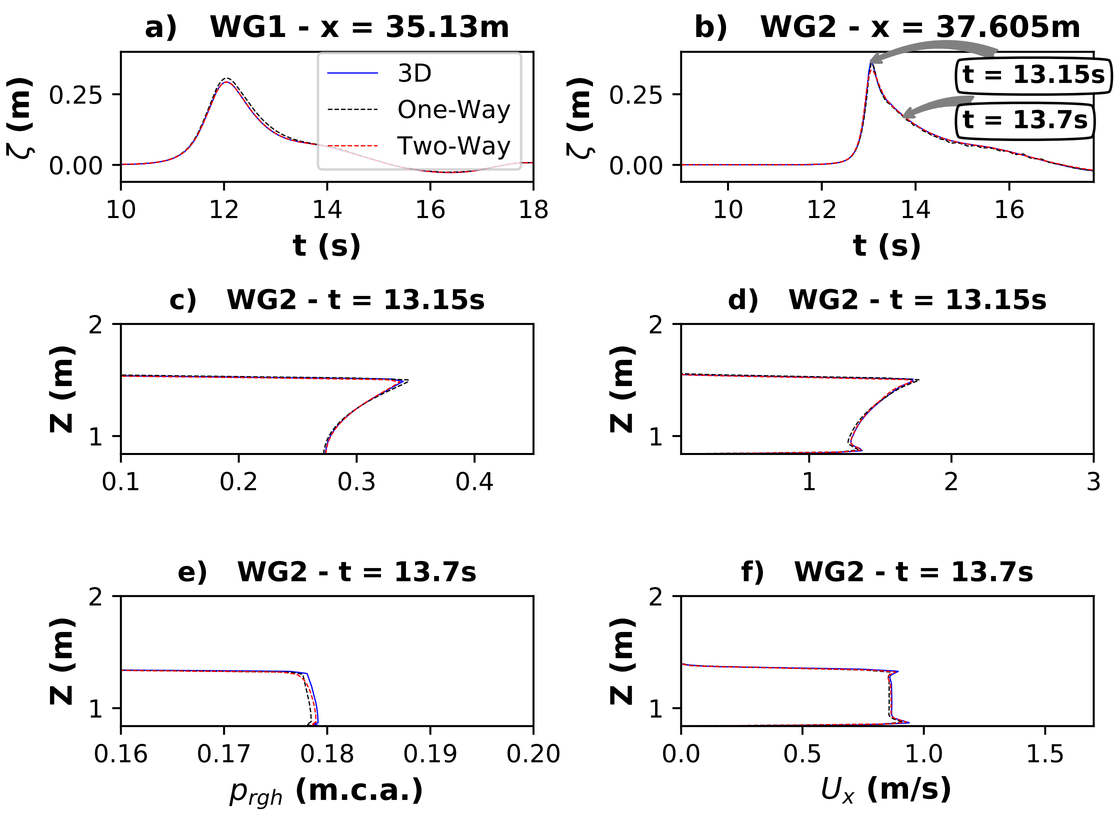

Figure 6: Free surface elevation comparison for a solitary wave propagating on a very shallow foreshore ($H = 0.25m$ and $h = 1.18m$). The blue continuous line represents the 3D case, the dashed black-line shows the one-way results and the dashed red-line represents the two-way results.

Good agreement is found when comparing the dynamic pressure (p_{rgh})(panel b) and e)) and horizontal velocity (U_x) (panels c) and f)). The peak pressure under a crest matches well the 3D solution for the two-way data (panel c), while small discrepancies are observed for the one-way results. A good agreement is also shown for $t = 13.7s$ (panel e) although a small deviation from the 3D solution is displayed for the one-way model.

A good match of the velocity profiles is also shown in Figure 6, panels d) and f) with a small overestimation by the one-way coupled simulation of the peak velocity calculated with the full 3D model at $t = 13.15s$ (panel d). Similar results are shown at $t = 13.7s$ (panel f) where a good correlation between coupled and full solutions is found. A small velocity overshoot appears close to the bottom during the deceleration phase (panel f) which probably is not physical as the boundary layer is not resolved. However, this case of study was only needed to demonstrate that the coupled and 3D models give similar results for wave propagation on a shallow foreshore. The velocity overshoot is related to numerical issues.

It is evident from the results that both the one-way and two-way couplings are capable of dealing with wave transformation over very-shallow foreshores. The coupled models are able to transfer information even for highly non linear waves. Wave transformation is well reproduced at the coupling location as well as in the far field ($x = 37.605m$) where both the free surface, dynamic pressure and velocities match well in space and time.

2.3 Three-dimensional flows under regular waves and focused wave groups

The following set of cases is devoted to test the effect of placing the interface at a location where waves are highly non-linear and a certain amount of the incoming energy is reflected back. This process is analysed in combination with three-dimensional effects in the near field, namely the breaking of waves on planar beach and wave interaction with a cylinder. These two layouts are shown in Figure 7 (panels a and b), the only difference being the presence of a cylinder in the near field. In both configurations an obstacle is placed in the 2D domain to increase wave steepness and non-linearity (H/L and H/h). The obstacle (Figure 7) induces an additional wave reflection from the 2D to the 3D domain precluding the use of one-way model as it does not allow considering bi-directional flows between the 2D and 3D domains. Consequently, only the two-way algorithm has been used. A highly reflecting beach (1:5) has been positioned in the 3D region to reflect incident waves and promoting the interaction with the coupling boundaries. As can be seen, panel b) displays the same layout as panel a) but in the former a cylinder inducing a three-dimensional flow has been placed in the surf zone. Three numerical simulations have been carried out for the layout in panel a) considering regular waves and a focused wave group, cases RW1, RW2 and WF1 in Table 4, respectively. One last simulation has been run to calculate forces on the cylinder under a focused wave group (WF2 in Table 4).

Regarding the numerical setup, an aspect ratio of 1 ($\Delta_x/\Delta_z = 1$) and of 12 cells per wave height have been used. The mesh has been refined around the cylinder ($\Delta_x = \Delta_y = \Delta_z = 0.005m$). The maximum Co has been set to 0.3 for all cases in Section 2.3. The stabilised $k-\omega$ turbulence model has been used. Table 4 presents a summary of the tests carried out including wave steepness and non-linearity for the regular tests and the wave focusing characteristics. The cylinder is centred along the y-axis of the 3D region and placed at $x_{cyl} = 26m$. $D_{cyl} = 0.1m$ is the diameter of the cylinder.

Figure 8 shows a comparison the of free surface evolution and the horizontal velocity field between the two-way coupled model and the full 3D simulation at WG9. For the sake of simplicity horizontal velocity profiles are displayed. A good fit is observed for the free surface elevation in the swash zone (panel a) although some discrepancies appear. The horizontal velocity profiles after the passage of the wave crests show a good correlation between the two-way and 3D results for all time instants considered (panels from b to e), although some discrepancies are observed. A good match for the maximum velocity is shown (panels from b to e).

Figure 9 shows the free surface along the numerical domain for $t = 50.9s$. In particular, the top panel spans to the entire domain whereas the bottom sub-plot shows a zoom at the coupling and near-field zones. The vertical scale (Z(m)) is magnified by a factor of 4 in order to better observe

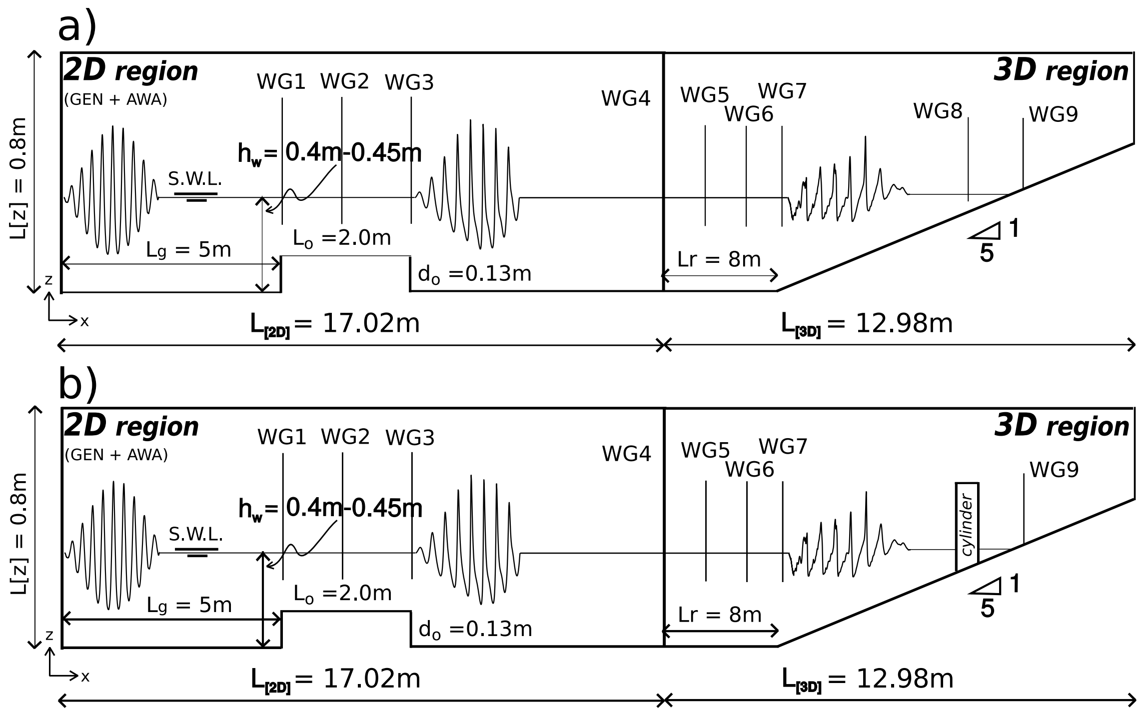

Figure 7: Sketch of the numerical simulation layouts.

the discrepancies between the 3D solution (black line) and the coupled two-way model (red-line). The cyan-line indicates the still water level (SWL). It can clearly be seen that, overall, a good match is found although very small local discrepancies are visible, which are possibly due to small 3D residual flow effects that cannot be transferred from 3D to 2D in the coupled model. Furthermore, the run-up oscillation obtained from the coupled model match the 3D solution very well.

Two additional simulations have been carried out considering a transient wave group as outlined in Table 4 (cases WF1 and WF2). A focused group shoaling on an obstacle inside the 2D domain and breaking on a planar beach in the 3D region is simulated as shown in panel a) of Figure 7. A second simulation was carried out considering the setup in panel b), that is including a cylinder.

Figure 10 shows the time evolution of the focused wave group together with the bound long-wave induced by the short waves. Two-way results are shown in dashred red-line while the 3D numerical data are displayed with blue-lines. The low-frequency motion (bound long wave) is magnified by a factor of 10. It can be readily observed that all signals match well. At gauge WG1, the bound long wave trough appears under the peak of the short wave group consistently with past research (Lara et al. (2011)). A small positive long wave is shown ahead of the group. The dynamic set-down is delayed with respect to the wave group when the shoaling process starts, from WG2 on. The time delay starts in the shoaling zone over the step (WG2) and increases as can be observed at WG3. Then wave reflection occurs and the delay is less apparent. The evolution of the infragravity wave is well reproduced using the coupled model. Small discrepancies are

	RW1	RW2	WF1	WF2
H**[m]**	0,12	0,1	0,1	0,1
h**[m]**	0,45	0,4	0,4	0,4
T**[s]**	3	3,5	-	-
H/L**[-]**	0,02	0,015	-	-
H/h**[-]**	0,27	0,25	-	-
f_c**[Hz]**	-	-	0,505	0,505
Δ_f**[Hz]**	-	-	10	10
N**[-]**	-	-	-	50
d_o**[m]**	0,13	0,13	0,13	0,13
Lo**[m]**	2	2	2	2
Lg**[m]**	5	5	5	5
x_{ccyl}**[m]**	-	-	-	26
D_{cyl}**[m]**	-	-	-	0,1

Table 4: Wave parameters for three-dimensional flows. Parameters d_o, L_o and L_g are shown in Figure 7. $x_{cylinder}$(m) indicates the x position of the centre of cylinder for the wave focusing simulation (WF1). N is the number of components used for the focused waves and f_c is the central frequency.

Gauge	X(m)	Gauge	X(m)	Gauge	X(m)
WG1	5.0	**WG5**	20.0	**WG9**	27.02
WG2	6.8	**WG6**	21.34		
WG3	8.0	**WG7**	22.21		
WG4	17.02	**WG8**	26.02		

Table 5: Location of surface gauges (see Figure 7).

observed in the swash zone. The coupled model appears to slightly over-predict the amplitude of the oscillations. However, the difference between 3D and coupled results is acceptable.

Figure 11 shows free surface and horizontal velocity comparisons at WG9. In general, a good correlation between the coupled and the 3D simulations is found. A good fit is observed for the free surface elevation in the swash zone (panel a) although some discrepancies appear. On average, a good correlation for the horizontal velocity profile is observed, qualitatively (panels from b to e), although some discrepancies are evident. The three-dimensional effects combined with high wave reflection are possibly the cause of the divergence in the results between the two-way and the 3D simulations.

Finally, Figure 12 shows the horizontal velocity field at the free surface elevation obtained with the coupled and 3D models. The upper panel displays a velocity snapshot calculated using the coupled simulation while the lower displays the 3D results. Horizontal (y-axis) and vertical (z-axis) scales are magnified by 8 and 4, respectively, in order to point out differences. A good agreement throughout the domain is observed.

To complete this first set of validation tests to assess the application of the coupled models, the force acting on a three dimensional structure under breaking conditions has been calculated, Figure 7, panel b). Forces are calculated from pressure and viscous stresses integration which are

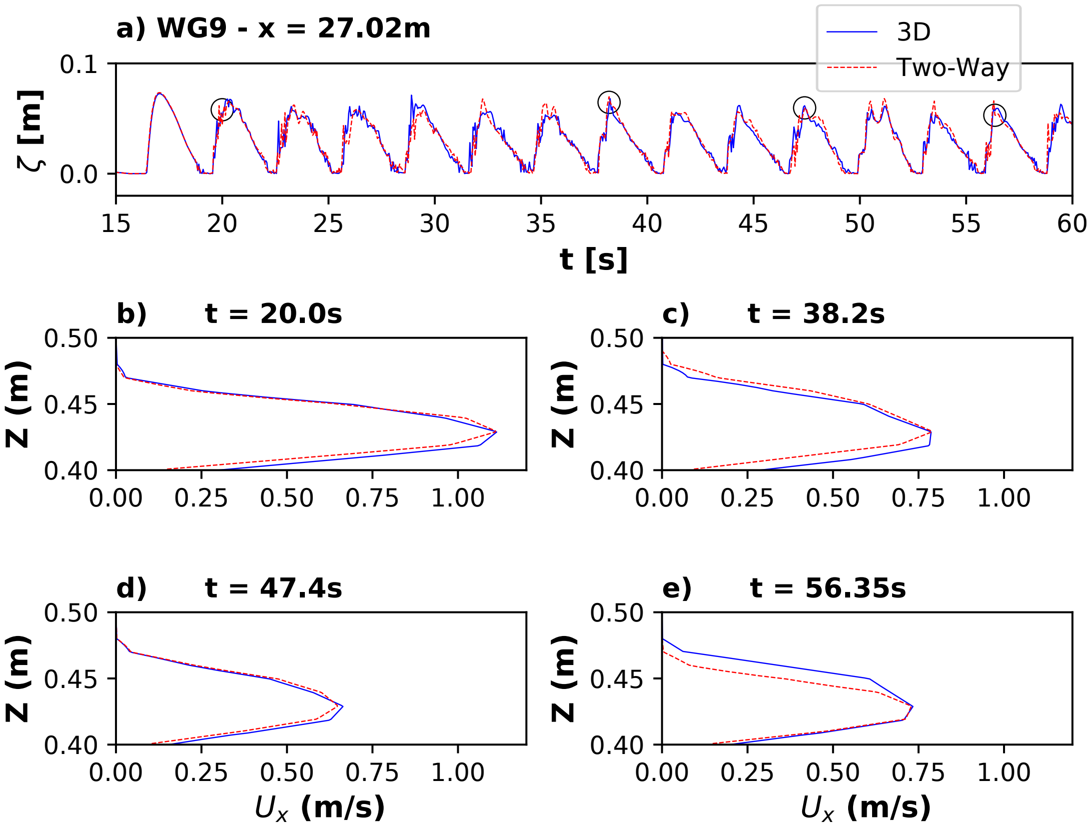

Figure 8: Case RW1: Comparison of free surface and horizontal velocity profiles between the two-way coupled model and the 3D simulation. Panel a) free surface time series at WG9. Panels from b) to e) horizontal velocity profiles at WG9.

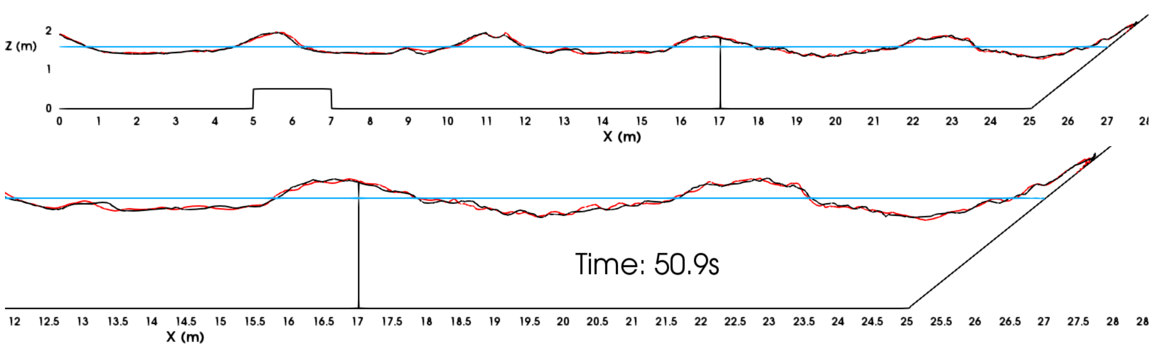

Figure 9: Case RW1: Wave profile along the numerical domain. Black and red lines show 3D and two-way coupled model results, respectively. In cyan the still water level is shown. The instant of time is $t = 50.9s$. The vertical scale (Z(m)) is magnified by a factor of 4.

a direct output of the RANS-VOF model.

Figure 13 displays the horizontal velocity field at the free surface level (panels a,b,d and e) and beneath the waves (panels c and f) at $t = 44.75s$ for both the coupled model (two upper

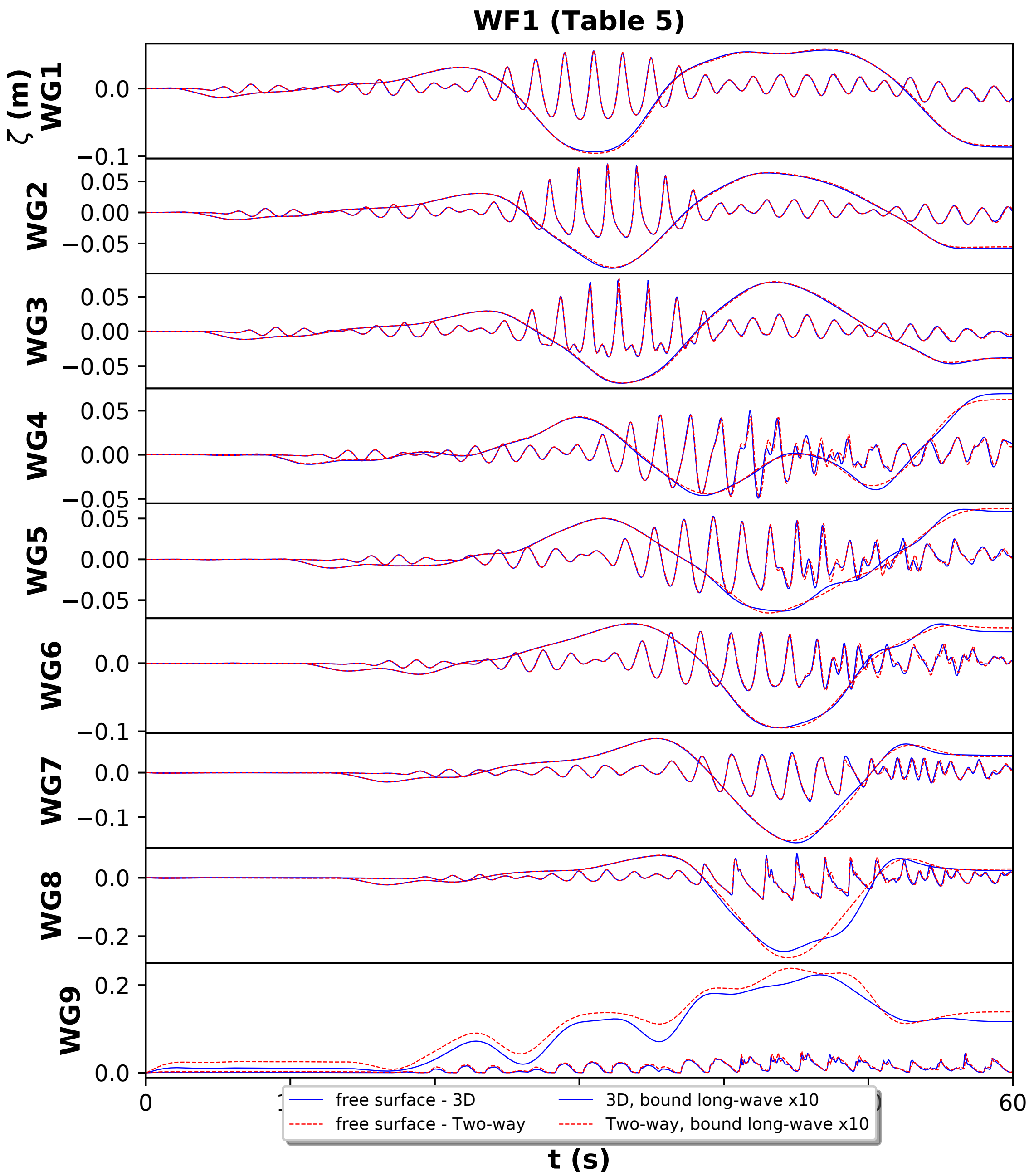

Figure 10: WF1: Free surface elevation time series. The bound long wave is displayed (magnified by 10) at gauges WG1 to WG9. Comparison between 3D and two-way results.

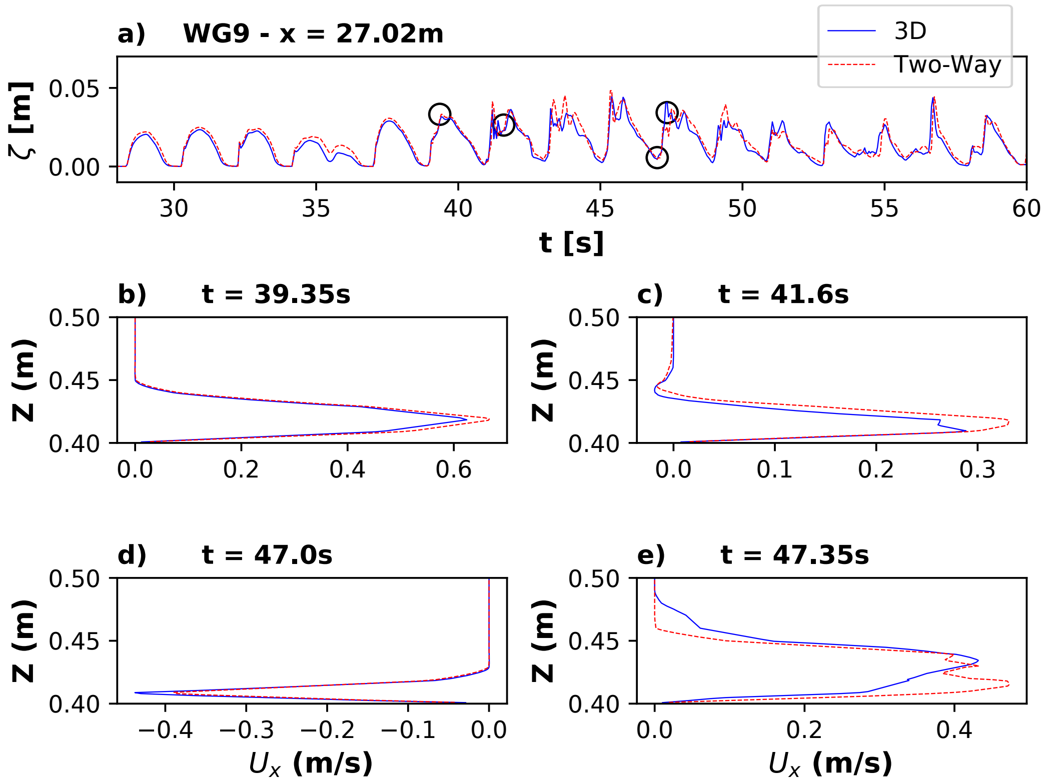

Figure 11: Case WF1: Comparison of free surface and horizontal velocity profiles between the two-way coupled model and the 3D simulation. Panel a) free surface time series at WG9. Panels from b) to e) horizontal velocity profiles at WG9.

panels) and the 3D simulation (two lower panels). From the inspection of the coupled model results (panels a, b and c) it can be observed that no three-dimensional patterns are present at the 2D-3D interfaces while strong 3D effects take place around the cylinder and along the sloping beach. Velocities at the coupled interface location are smooth as already shown earlier in the paper. The model was shown to be robust and stable to simulate such a complex case, i.e. second order wave generation and multiple structures (beach, cylinder and shoaling-step). Similar results are presented in the lower panels of Figure 13, i.e. panels d), e) and f) (3D results). The plunging breaker occurs approximately at the same position in space and time for both the 3D and the coupled simulations (panels from a to f). A good agreement is found for the velocity field around the cylinder comparing the full and coupled models. A good correlation is also observed for the horizontal velocity field from the cylinder to the coupling position ($x = 17.02m$). Finally, also the run-up oscillation seems to agree well (panels b and e) although small discrepancies are visible. By observing panels c) and e) it can be noted that a good correlation for the velocity profiles beneath the waves is obtained for the two-way coupled model (panel c) and the 3D simulation (panel e). Velocities at the plunging breaker are comparable although some discrepancies are visible. Small deviations can always occur due to the combination of three-dimensional effects and high wave reflection. In the 3D model small three-dimensional effects can propagate throughout the domain while in the two-way model are neglected at the coupled interfaces.

Next, Figure 14 shows the horizontal force calculated on the cylinder. A good can be noted throughout the simulation time for the impact of the focused wave group. Both positive and negative peaks are well-simulated providing evidence that the coupled model can replace the use of the full 3D simulation when three-dimensional effects occur (and more or less confined) in the near-field. A similar result was already obtained by El Safti et al. (2014) when simulating forces induced by focused waves on a cylinder by using the 2D-3D one-way coupled model. However, the present approach allows a considerable decrease of the numerical domain compared to the work by El Safti et al. (2014) as neither overlapping zones nor relaxation methods are needed. In addition, the models proposed herein also allow considering a two-way coupled scheme which is essential for most applications. It is evident from the results that the coupled model has proven to be highly accurate in reproducing nearshore hydrodynamics considering complex geometries and structures also including second order wave generation.

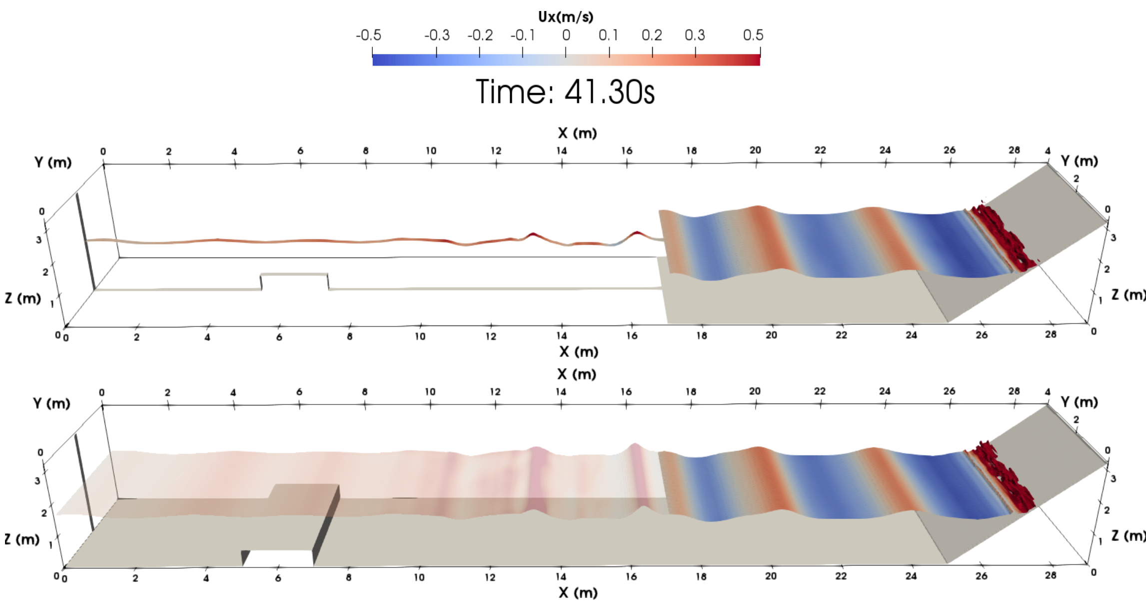

Figure 12: Case WF1: Snapshots of the horizontal velocity at the free surface (Ux[m/s]). The two-way coupled model (upper panel). Full 3D model (lower panel).

2.4 *Wave interaction with a perforated breakwater*

Perforated breakwaters or caissons, frequently named as Jarlan-type caisson breakwaters (JTCB) after the pioneering work presented in Jarlan (1961), are typically designed to reduce wave reflection. JTCB have received a lot of attention in the past mainly focused on the development of accurate analytical, experimental and numerical models aiming at understanding and predicting the complex interaction mechanisms involved. As the geometry of the perforated caisson increases complexity it may not be possible to obtain explicit analytical solutions. In addition the use of

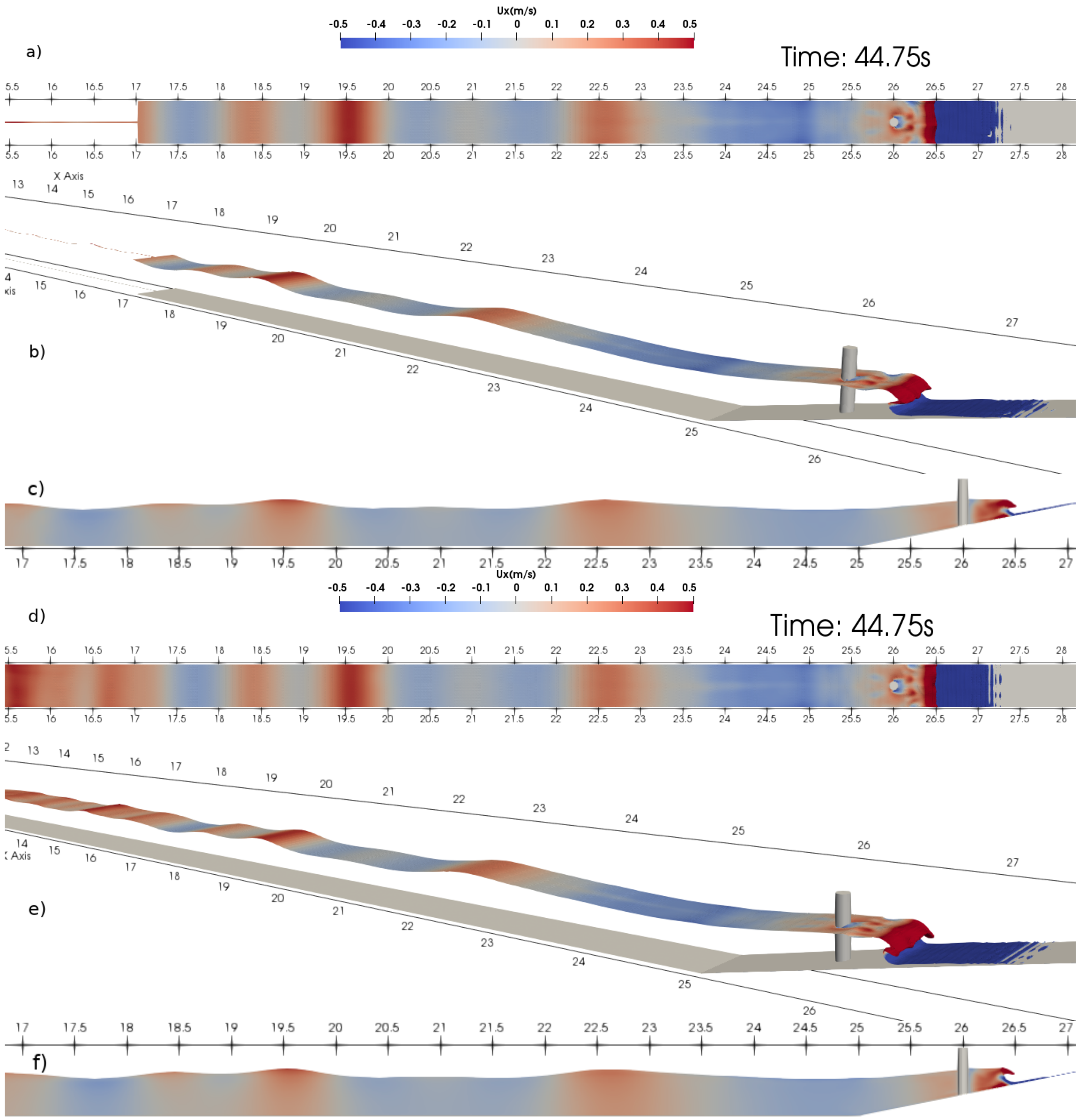

Figure 13: Case WF2: Snapshots of the horizontal velocity at the free surface and beneath the waves (Ux[m/s]). Two-way coupled model (panels a, b and c). Full 3D model (panels d, e and f).

physical models can be very expensive if several configurations need to be tested. In these circumstances, the CFD models represent a reliable tool to characterise the response of perforated breakwaters under wave action (Wang et al. (2019)). Wang et al. (2019) carried out 2D and 3D simulations and compared results against experimental tests. The effect of the perforated caisson was introduced in the 2D simulation as an equivalent porous media using Volume-Average Reynolds-Average Navier-Stokes (VARANS) formulation. The main conclusion was that in com-

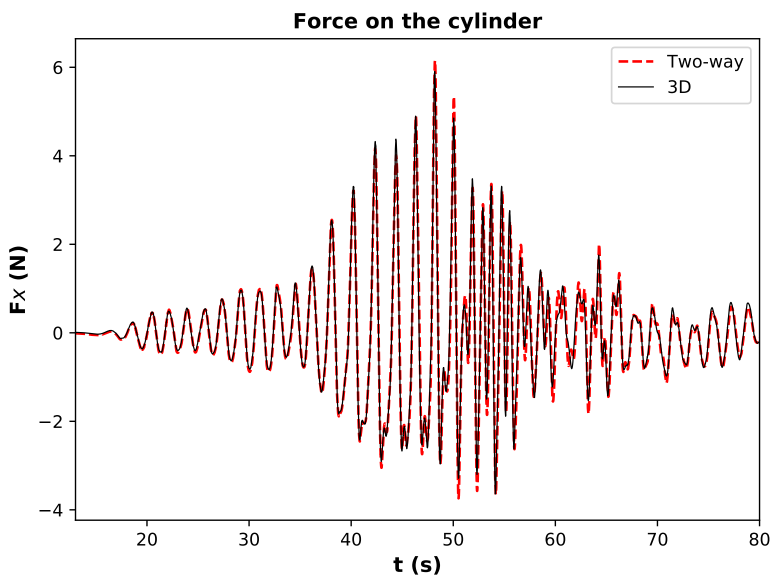

Figure 14: Case WF2: Horizontal force acting on the cylinder. The centre of the cylinder is placed at $x = 26m$.

parison with laboratory data the 3D models were able to predict the wave reflection coefficient while 2D simulations showed important disagreement with experimental results. This was partly attributed to the elimination of the vertical part of the tested structure and partly to the overestimation of the equivalent porosity. Wave load results also showed that 3D simulations agreed with the experimental results whereas 2D models deviated from laboratory data. Unfortunately, the computational time of full 3D simulations is tremendously expensive and for these reason the 2D-3D couplings may help to reduce computation efforts while keeping a high accuracy.

In the experimental campaigns of Wang et al. (2019) the Jarlan-type caisson breakwater (JTCB) was tested in a 56m long, 0.7m wide and 1.0m high wave tank. The extension of the experimental area was 35m, from the wavemaker to the front wall of the JTCB. The JTCB, characterised by square-apertures, was partially filled with porous material inside the wave chambers. The experimental layout will not be described in detail here as it is extensively documented in Wang et al. (2019).

Regarding the 2D and 3D numerical simulations (Wang et al. (2019)), the dimensions of the vertical breakwater and the foundation remained unchanged while a shorter numerical wave tank was considered in order to reduce computational time. The 2D simulations were carried out considering a $5 \cdot L + L_0$ long domain, where L is the wave length and $L_0 = 1.0m$. The numerical domain was shortened for the 3D simulations up to $3 \cdot L + L_0$ to reduce the computation time. In the 3D regions of the coupled simulations 17 cells were defined in the spanwise direction ($\Delta_y = 0.04m$). The refined cell is 0.005m long and 0.0025m high and 0.01m wide. The same cell sizes in length (x) and height (z) of the mesh II are used as reported by Wang et al. (2019). A summary of the mesh sensitivity analysis performed by Wang et al. (2019) is shown in Table 6. The maximum Co

number has been set to 0.75 for all simulations of wave interaction with the JTCB (Section 2.4). The stabilised $k - \omega$ turbulence model has been used.

Cases	Δ_x	Δ_z	**AR**	n^o cells
I	L/146	H/16	2:1	116.800
II	L/292	H/32	2:1	204.400
III	L/584	H/64	2:1	554.800

Table 6: Mesh sensitivity analysis by Wang et al. (2019). AR is the aspect ratio (Δ_x/Δ_z).

Wang et al. (2019) used mesh II in Table 6 for the 2D simulations whereas mesh I was applied for 3D cases to reduce the computational time. The hydrodynamic conditions used were shown in Table 3 of Wang et al. (2019).

In the present work, first, the coupled simulations will be carried out first considering the following wave characteristics: wave height $H = 0.08m$, wave period $T = 1.4s$ and water depth $d = 0.4m$ (H/d = 0.2, H/L = 0.033). Additional simulations are carried out with B/L ranging from 0.062 to 0.25, where B is the length of the wave chamber (x-direction). The present simulations are based on the mesh sensitivity analysis performed by Wang et al. (2019), so mesh II was used for all simulations. Moreover, the length of the numerical domain is taken to be equal to the actual experimental area. The front wall of the JTCB is located 35m away from the numerical wavemaker. Two different 2D-3D couplings have been considered. The first is characterised by a small 3D region placing the coupling interfaces at 0.5m from the front wall, while this dimension is increased up to 2.78m for the second option. A comparative sketch is shown in Figure 15. The main objective is to validate the coupled models against laboratory data and the 3D simulations developed by Wang et al. (2019). Furthermore, the influence of the length of the 3D domain is assessed. In the first configuration (Figure 15, left panel) the free surface gauges used to calculate the reflection coefficients are located inside the 2D domain whereas for the second lay out (Figure 15, right panel) the gauges are placed within in the 3D region. The dimensions of the numerical domains used to carry out the coupled simulations are summarised in Table 7.

The third simulation in Table 8 has been run using both the ”small” (left panel of Figure 15) and ”large” (right panel of Figure 15) coupled models, while for other cases only the ”small” coupled model has been used. Table 8 outlines the main features of the numerical simulations.

The two-way coupled model is needed to assess the wave reflection coefficient. It allows to:

- simulate the same wave reflection as in the laboratory setup
- consider a small 3D domain because the wave gauges for wave reflection can be placed inside the 2D region (while for the one-way model the wave gauges for calculating wave reflection have to be placed inside the 3D domain).

The reader is referred to Figure 7 and 13 of Wang et al. (2019) for the position of the pressure transducers and for the layout of the numerical velocity gauge, respectively.

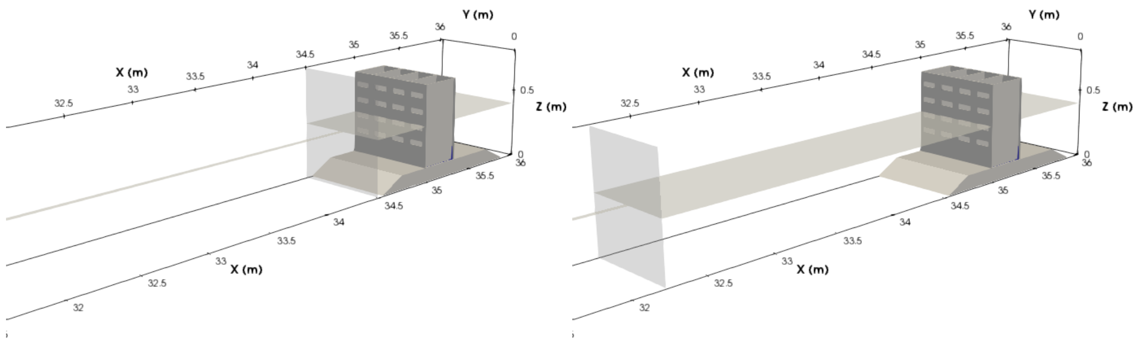

Figure 15: Scheme of the 2D-3D coupled simulations carried out for the two-way simulations. Left: small coupled simulation. Right: large coupled simulation (dimensions in Table 7).

Coupled simulation	**X_{2D}(m)**	**Y_{2D}(m)**	**Z_{2D}(m)**	**X_{3D}(m)**	**Y_{3D}(m)**	**Z_{3D}(m)**
small	34.5	0.04	0.8	1.55	0.7	0.8
large	32.22	0.04	0.8	3.8	0.7	0.8

Table 7: Dimensions of the numerical domains adopted for the coupled simulations.

Coupled simulation	**h (m)**	**H (m)**	**T (s)**	**L (m)**	**H/L[-]**	**H/h[-]**	**B/L[-]**
small	0.4	0.08	0.9	1.22	0.066	0.2	0.25
small	0.4	0.08	1.2	1.94	0.041	0.2	0.155
small - large	0.4	0.08	1.4	2.39	0.033	0.2	0.126
small	0.4	0.08	1.6	2.84	0.028	0.2	0.106
small	0.4	0.08	2.1	3.91	0.02	0.2	0.077
small	0.4	0.08	2.55	4.84	0.017	0.2	0.062

Table 8: Wave characteristics used in the two-way coupled simulations.

2.4.1 Wave reflection coefficient

The wave reflection coefficient ($\mathbf{k}_r$) is probably the most important factor considered in the design of a JTCB as it is to be minimized usually to reduce wave reflection in navigation areas. Figure 16 shows experimental and numerical wave reflection coefficients plotted against the ratio B/L. Black circles and triangles refer to the coupled simulations (small and large, respectively); black-squares show the experimental data; grey triangles and diamonds refer to the 2D and full 3D simulations carried out by Wang et al. (2019), respectively. Note that for different values of B and different wave conditions (L) the same values of B/L can be obtained (e.g. Laboratory, 2D and 3D data of Wang et al. (2019)).

The first conclusion is that the coupled simulations give results close to the experiments with an error below 10%. The "small" and "large" coupled models give similar results (B/L=0.126). The setup with the small 3D domain is capable to capture 3D effects and demonstrates that they are confined close to the front wall. Wave gauges used to calculate wave reflection can thus be placed indifferently in the 2D region or in the 3D domain. Proven that both coupled models give similar results, five additional simulations have been carried out varying the ratio B/L from 0.062 up to 0.25 for the small coupled layout.

It can be readily observed that the coupled model leads to reasonable results for the entire range of B/L analysed. Compared to the experimental data, the error in the estimation of $\mathbf{k}_r$ ranges from 3.8% (B/L=0.126) to 9% (B/L=0.062). $\mathbf{k}_r$ increases for low ratios of B/L, reaches low values for 0.12 < B/L < 0.205, then increases again.

For B/L=0.126 the coupled models seem to give better results than the full 3D simulations performed by Wang et al. (2019) and probably as a consequence of the more refined mesh used in the present work. Indeed, in order to reduce the computational time, Wang et al. (2019) had carried out the 3D simulations applying the coarsest mesh included in the mesh sensitivity analysis. In the present work there was no need to further reduce the computational time, as the 2D-3D approach already allowed to strongly reduce the numerical domain. It can be noted that $\mathbf{k}_r$ does not present the minima of the wave reflection coefficient for B/L close to 0.25 compared to the theoretical analysis for one-chamber breakwaters (Fugazza and Natale (1992)).

Besides, Wang et al. (2019) pointed out that the results of the 2D simulations diverged from the laboratory data and the full 3D simulations. The 2D results under-estimate the reflection coefficients, especially for low ratios B/L.

As a conclusion, results of the coupled simulations are reliable as they show a good match with both the experimental and full 3D data. Due to a more efficient computational performance, in the following, results of the small coupled simulations are shown only.

2.4.2 Velocity measurements

Concerning the velocity field, only numerical results (2D and 3D) were provided by Wang et al. (2019) (see Figure 19 of Wang et al. (2019)). In particular gauges V1 and V2 placed on both sides of the front wall are used here in order to compare velocities where 3D effects are dominant. V1 is located at the sea-side and V2 is placed inside the wave chamber (Figure 13 of Wang et al. (2019) for reference). Horizontal (U) and vertical (W) orbital velocities are shown in Figure 17. The dashed blue and red lines refer to the 2D and 3D simulations while black lines display the results of the coupled model. Overall, a good match between the full 3D and coupled simulations is shown. At the sea-side gauge it can be seen that both the horizontal and vertical velocities match the 3D solution. Particularly, the vertical velocity is slightly over-predicted by the coupled model but with small differences, whereas the 2D simulations overestimate the velocity at the passage of the wave crests. A good correspondence between the coupled and 3D simulations is found for the gauge V2 inside the chamber. The velocity peaks are captured (U) although flatter troughs were obtained with the full 3D simulations. Here it can be noted that the 2D model is unable to predict the positive velocities showing a phase lag. Finally, some discrepancies arise for the vertical velocity inside the chamber although results can be considered to be acceptable.

2.4.3 Pressure measurements

It is key to check that the numerical models are able to estimate wave pressure to accurately characterise wave loads on the JTCB. Several pressure gauges located at the front wall (sea-side

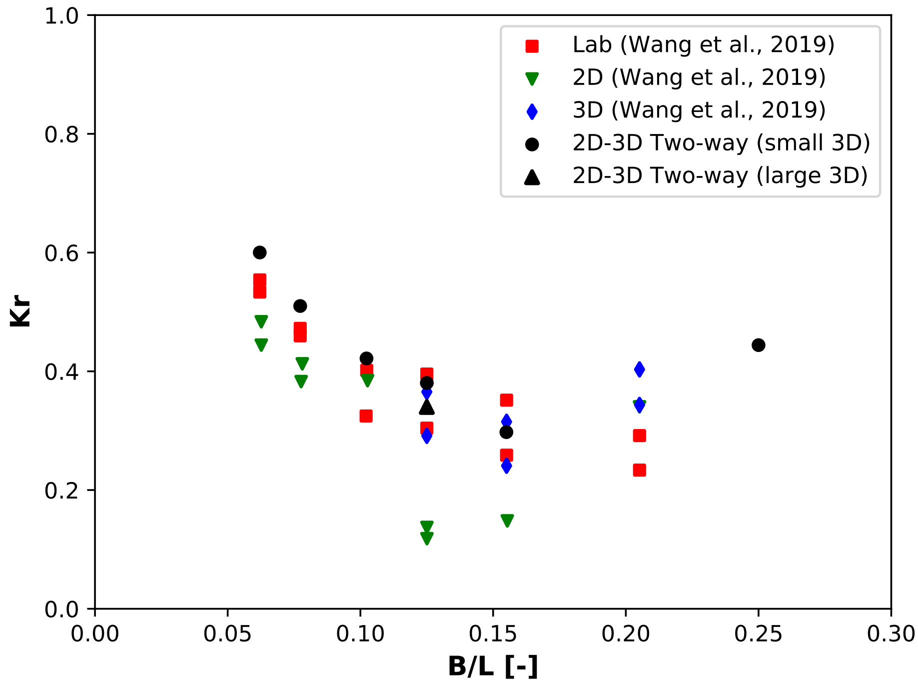

Figure 16: Wave reflection coefficients Kr.

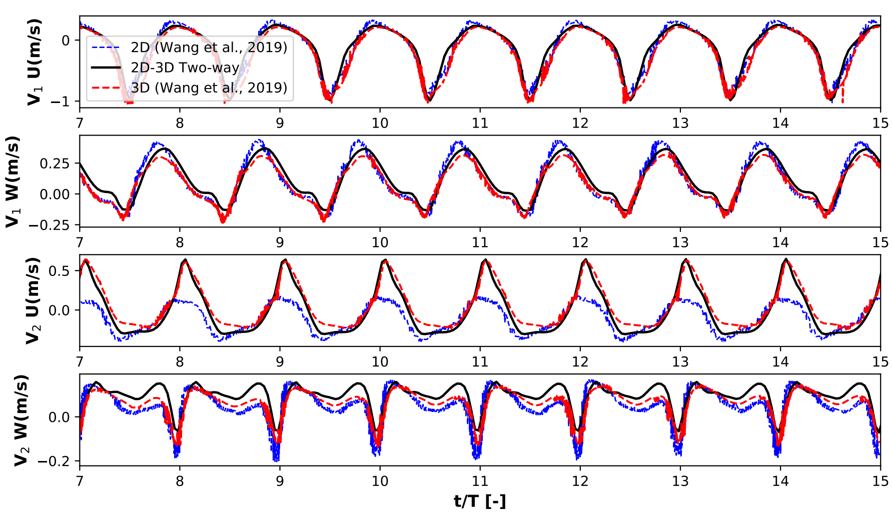

Figure 17: Horizontal (U) and vertical (W) velocities measured at the gauges V1 and V2 defined by Wang et al. (2019).

and inside the chamber) and at the bottom of the caisson are displayed. Forces are typically calculated by integrating pressure over the surfaces. Consequently, calculating the hydrodynamic pressure with a good accuracy is crucial. Figures 18 and 19 display comparisons between the coupled model (black), laboratory (red) and pure 2D simulations (blue). An excellent match between laboratory and coupled model results is shown for each gauge placed at the sea-side of the front wall. Both positive and negative pressure peaks are reproduced at different depths. Gauge 4 is placed just above the still water level only measuring positive peaks. In opposition to Wang et al. (2019) who noted a mismatch between 3D and laboratory data, the results here are satisfactory. Experimental and coupled model data are well-correlated although with very small deviations. The 2D results show discrepancies with the laboratory and coupled models, demonstrating that the 2D approximation is not suited for this application, even if the equivalent porous media is accurately set. Similar results are shown inside the chamber, particularly when the water level within the chamber decreases. A mismatch of the negative pressure is obtained when applying the 2D model, whereas the coupled simulation is extremely precise in the estimation of maximum and minimum values as well as when high-order harmonics appear. A good match is also obtained at the bottom gauges inside the chamber (gauges 11 and 12), proving that the coupled model accurately simulates the wave motion inside the chamber without additional energy loss due to the coupling scheme.

Figure 20 compares the hydrodynamic pressure on the front wall (gauges from 1 to 4) of the caisson obtained by the small and large coupled simulations defined in Table 7. A good match in the maximum and minimum values of the hydrodynamic pressure is obtained throughout the simulation and no damping is observed although a small delay is found among the signals. This effect which is known in literature as ”lose coupling” (Martínez-Ferrer et al. (2016)) leads to a delay between the left and right side solutions (2D and 3D domains) in segregated couplings. However, the results are very satisfactory.

2.4.4 Force on the perforated wall

The total horizontal force acting on the perforated front wall is calculated from the coupled model results. Results of small and large 2D-3D simulations (Figure21) are plotted together. Results are presented without being filtered in order to allow a detailed observation of the differences between approaches. The comparison between the coupled and 3D data is also shown in Figure21 (upper and lower panels). Both coupled models (“small” and “large”) provide almost the same values for the maximum and minimum peaks of the inline force. In addition, the observed waveform of both cases is almost equal. A small phase-lag between signals (loose coupling) occurs. It can be observed that the phase-lag among signals varies in time comparing the two coupled models and the 3D results. This indicates that the loose coupling takes place for both numerical setups, i.e. ”small” and ”large” two-way coupled models, but again it does not affect the results significantly showing the high potential of the model coupling technique presented here.

2.4.5 Pressure comparison between one-way and two-way couplings

The first case in Table 8 has also been run in one-way mode in order to explore the capability of the model for the cases where the three dimensional flows take place close to the coupled in-

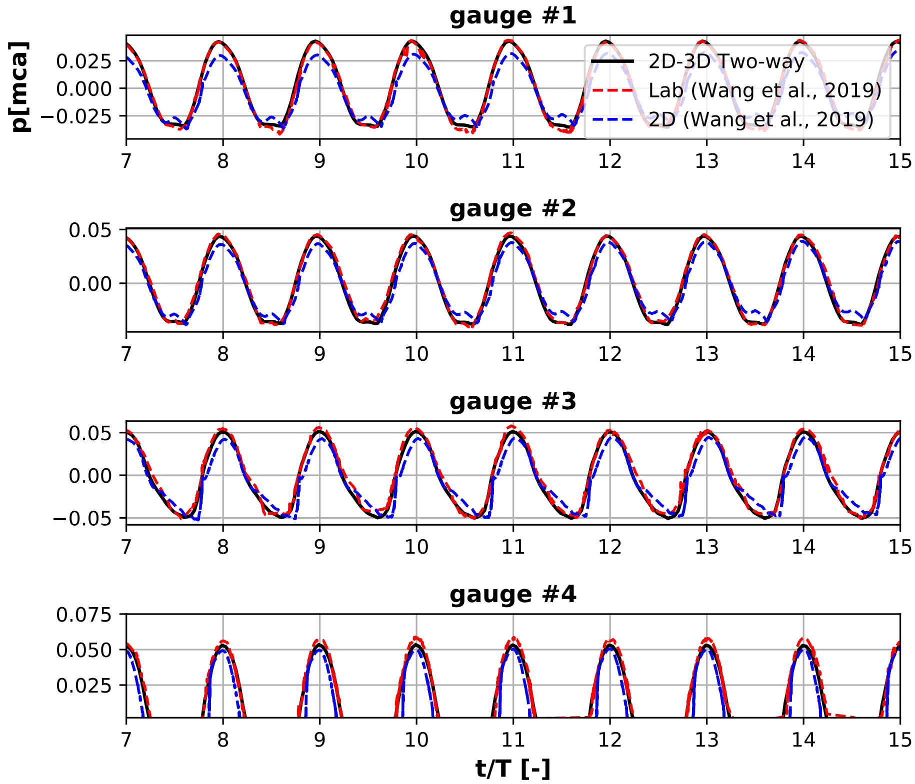

Figure 18: Comparison of the dynamic pressure field at the front wall between the small (black line) and the large (dashed-red line) coupled models. Gauges 1 to 4 are located at the front wall (sea-side).

terfaces. This simulation has been carried out in 3D as well, in order to analyse which coupling performs better for such a complex case. Figure 22 shows the results of dynamic pressure at the front wall of the breakwater. It can be observed that the one-way model gives acceptable results for all gauges although a small over-prediction of the pressure is shown, particularly for gauges 1 and 4. No phase lags are observed among signals. The two-way model appears to give better results than the one-way coupling compared to the 3D simulation.

2.4.6 3D results

Figure 23 shows the velocity field (U_x) at the free surface, and snapshots of the three dimensional flow through the perforated caisson. Small differences in the contour plot can be observed comparing the small (left) and large (right) coupled layouts. The differences are mainly due to very small phase lags between solutions ("loose coupling"), although the models have been proven to be highly accurate in calculating pressure, velocity fields as well as in estimating the wave reflection coefficient. The lower panels show the impact of a wave crest (t/T=12) followed by a wave trough (t/T=14.6). At t/T=12 the wave crest reaches its maximum, the flow into the chamber is finishing and the wave run-up at the bottom wall of the chamber occurs. The flow inside the wave chamber varies along the span-wise and wave directions. The water level inside the chamber is

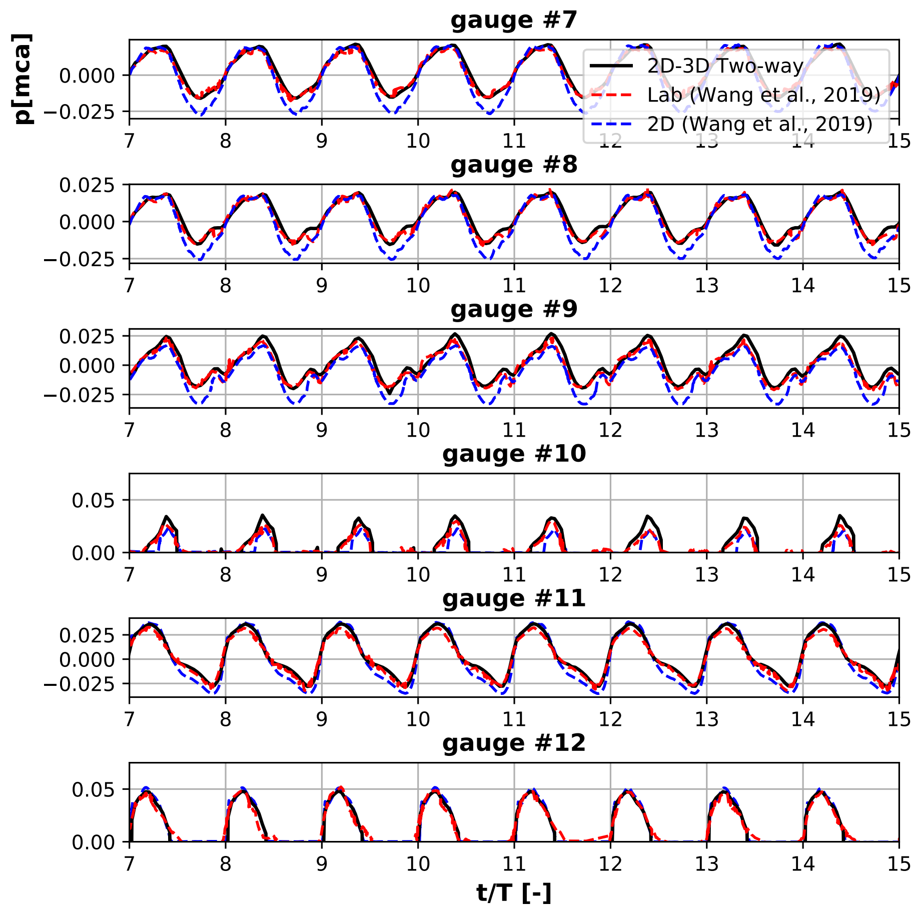

Figure 19: Comparison of the dynamic pressure field at the front wall between the small (black line) and the large (dashed-red line) coupled models. Gauges 7 to 10 are located at the front wall (inside the chamber). Gauges 11 and 12 are placed at the bottom wall inside the wave chamber.

lower than the wave crest as the wave can only partially penetrate the front wall. The strongest 3D effects occur during the outflow of the chamber. At t/T=14.6 the water level inside the chamber decreases and a complex 3D pattern appears close to the holes of the front wall.

Finally, Figure 24 shows a comparison of the velocity field beneath waves for the one-way, two-way and 3D simulations carried out in the present work. A snapshot when high wave reflection occurred is here shown in order to demonstrate the potentiality of the couplings. First, it can be seen that the two-way model shows a velocity field similar to the full 3D simulations, although small discrepancies are observed. Deviations may due to small 3D effects neglected at the two-way coupled interfaces, but however, the wave shapes appear to be correctly reproduced. The one-way model obviously displays different results as the reflected waves are absorbed at the 3D interface (x=34.5m). It can also be noted that the wave are not in phase with the 3D simulation, but it is due the different lengths of the computational domains. The velocity field at the interface is smooth, and it can be observed a uniform velocity profile (positive) close to x=34.5, which is induced by

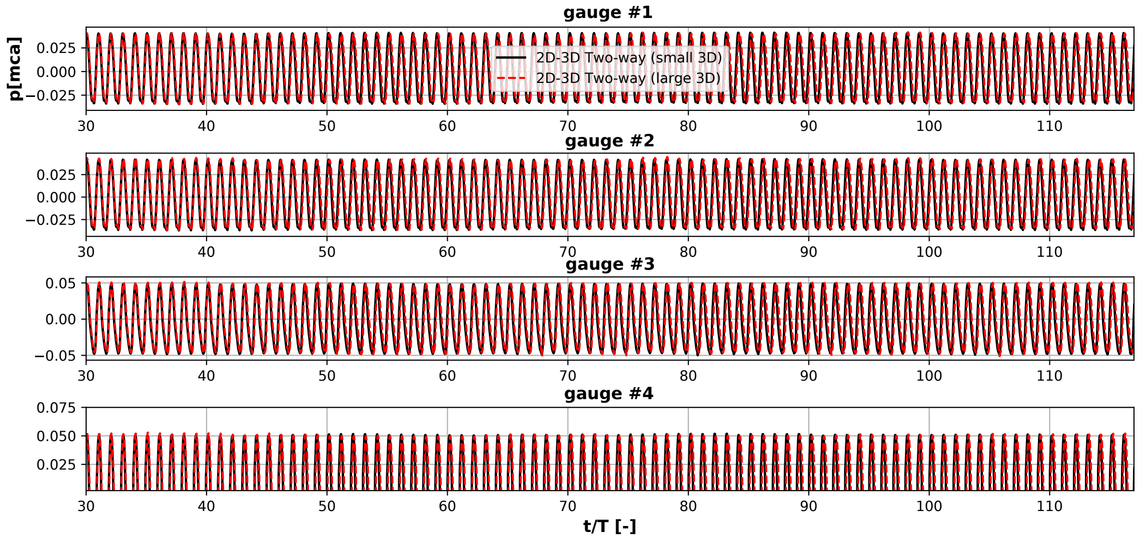

Figure 20: Comparison of the dynamic pressure on the perforated front wall (sea-side) between the small (black line) and the large (dashed-red line) coupled models.

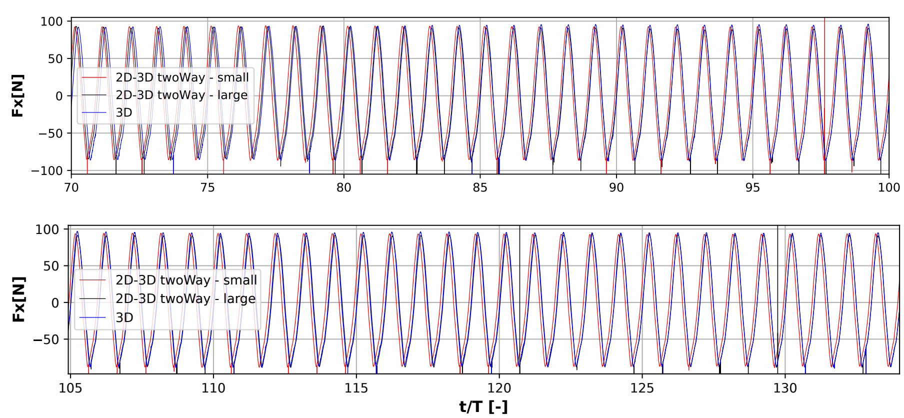

Figure 21: Horizontal force integrated on the front wall of the JTCB.

the active wave absorption based on the assumption of shallow water theory. Although the the small distance between the front wall of the breakwater and the coupled interfaces, the one-way model demonstrated a good capability in predicting pressure at the structure as shown in Section 2.4.5.

3 Concluding remarks

The implementations presented in Part I (Di Paolo et al., Part I, submitted) have been applied for practical cases where the three-dimensional effects are dominant (confined) in the near-field. From the results it is found that the 2D-3D modelling is reliable for all the cases analysed.

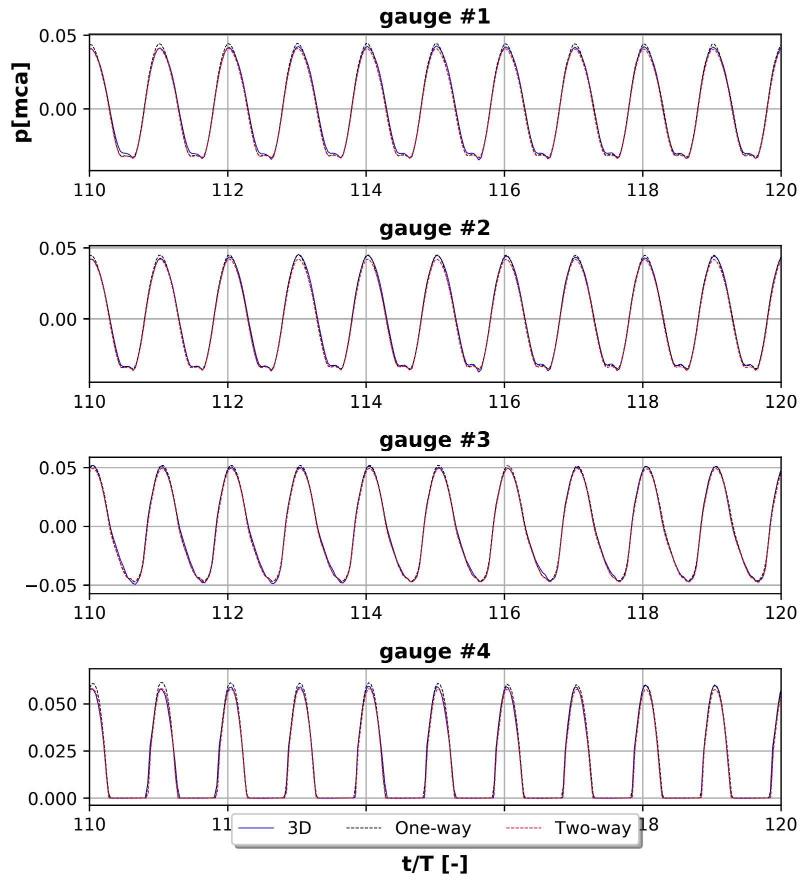

Figure 22: Pressure comparison at the front wall between the coupled (one-way and two-way) and 3D simulations carried out in the present work. All signals are synchronised to better compared the results, as different spatial domains are used, especially for the one-way and two-way setups.

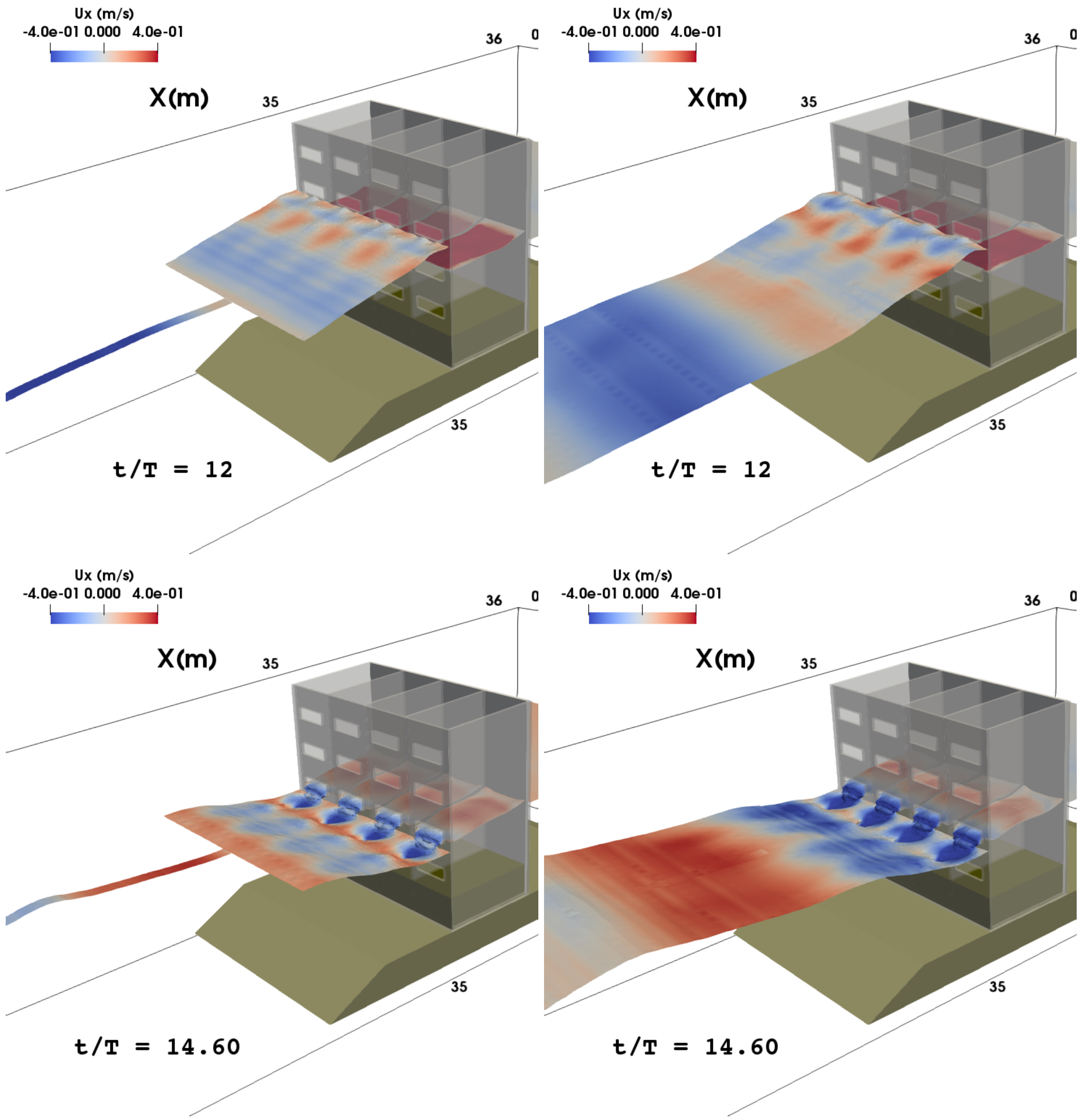

Figure 23: Snapshots of the velocity field at the free surface. Comparison between ”small” (left panels) and ”large” (right panels) two-way coupled simulations.

The methodology is suitable for regular and irregular waves, also considering long-waves induced by focused wave groups. The 2D-3D approach, here used to model a shallow foreshore, breaking waves on a planar beach, wave impact on a cylinder and wave interaction with a perforated breakwater can be extended to those cases where waves impact normally on three-dimensional structures and the 3D effects take place in the near field. It is always recommended to test a preliminary setup of the coupled simulation in order to check that 3D effects are enclosed within the 3D domain. This is however an easy task as the coupled model is computationally

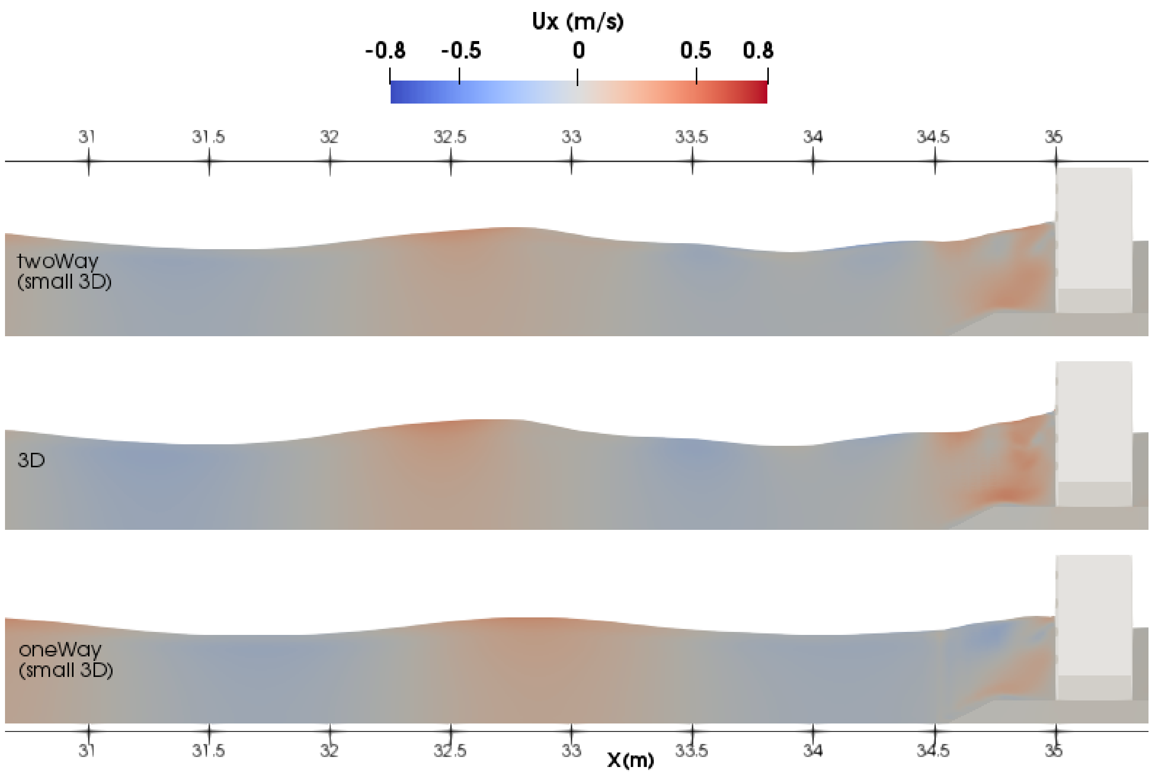

Figure 24: Velocity field beneath the waves (plan x-z, y=0.25m). Comparison of one-way, two-way and 3D simulations carried out in the present work. The coupled interfaces are located at x=34.5m.

Case	$\mathbf{CPU}_{3D}$ (d-h)	$\mathbf{CPU}_{1way}$ (d-h)	$\mathbf{CPU}_{2way}$ (d-h)	$\mathbf{n}_{speed}$ $_{3D-1way}$	$\mathbf{n}_{speed}$ $_{3D-2way}$	$\%$ $_{3D-1way}$	$\%$ $_{3D-2way}$	time (s)	Co	nProcs	two-way stab
RW	24d	15.3d	14d	1.57	1.71	36.3	41.7	180	0.1	8	-
IW1	40d	26d	20d	1.54	2	35	50	3600	0.1	8	active
IW2	27d	16d	22d	1.69	1.23	40.7	18.5	3600	0.1	64	active
Shallow foreshore	63h	18.9h	33h	3.33	1.91	70	47.6	20	0.1	8	active
WF1	112.2h	-	23.36h	-	4.8	-	79.2	80	0.3	8	active
WF2	182.4h	-	29.2h	-	6.25	-	84	80	0.3	8	active
JTCB small	111h	61h	59.1h	1.82	1.88	45	46.8	200	0.75	8	active
JTCB large	-	-	73h	-	-	-	-	200	0.75	8	active

Table 9: Computational speed-up obtained for the cases simulated.

cheap compared to the 3D simulations.

Moreover, it is of key importance to correctly set the numerical parameters of the simulations, particularly the cell aspect ratio and the Co. A low Co (e.g. 0.1) and a small cell aspect ratio (e.g. 1.0) may be needed in the most challenging cases. Lowering the aspect ratio and Co leads to a better estimation of the wave velocity profile along the water depth and a correct advection of the fluid through the entire domain and especially at the water/air interface, avoiding unphysical wave hydrodynamics. Such as, a low Co (0.1) and aspect ratio (1.0) were needed to correctly generate the target wave height for the irregular-wave simulations (Section 2.1). The same numerical parameters were needed to carry out the wave propagation on a shallow foreshore (Section 2.2). A small aspect ratio (1.0) and Co (0.3) were also required to obtain good results for three-dimensional flows under regular and focused waves (Section 2.3), while, for the last case of study (Section 2.4) a larger Co and aspect ratio allowed to obtain a good match between experimental and numerical (coupled models) results. For the case in Section 2.4, the use of larger Co and aspect ratio was balanced by a highly refined mesh, especially around the structure.

The 2D-3D modelling, also validated with a complex laboratory experiment of wave-structure interaction including fixed structures and porous media, has proven to be stable and accurate under several hydrodynamic conditions and for different locations of the coupled interfaces.

An asset of the 2D-3D approach is that it allows to carry out extensive numerical tests of medium and large spatial-scale simulations with a reasonable computational time. The ratio of computational acceleration (n_{speed}) and the computation load saved (%) are given in Table 9. CPU_{3D} and $CPU_{coupled}$ are the execution time of the 3D and the coupled models, respectively.

The main conclusion is that the coupled models allow to speed-up the simulations by a factor in the range of 1.54 and 6.25 depending on the case analysed. The long time series of regular and irregular waves, due to the small aspect ratio (AR=1) and Coruant number (Co=0.1) resulted in very expensive computational time, even using the coupled models. Note that in this case (ideal case) a very long 3D domain was defined in order to test the couplings. In realistic applications (e.g. JTCB) the sizes of the 3D region are generally smaller. Concerning the last case analysed, i.e. wave-JTCB interaction, it is shown that the computational cost is limited to approximately 2.5 days to complete a 200-second simulation using 8 cores only.

The methodologies proposed are not only helpful for wave interaction with cylinders or perforated caissons but can also be used to analyse the hydraulic performance of breakwaters integrated within WECs (vertical or rubble mound) or to determine the response of floating structures.

2D-3D RANS-LES modelling is also possible and could improve the accuracy in simulating breaking waves and impacts on structures at a reduced cost compared to full 3D simulations.

From the results obtained it can be concluded that the 2D-3D couplings proposed: (i) drastically reduce the computational time required by the full 3D simulations and (ii) give an accuracy comparable to the full solution and to laboratory data for the range of validation The methodology is ready to be used in a variety of realistic coastal and offshore applications including floating structures.

Future work will focus on the exploitation of the methodology and the inclusion of more physics (i.e. other models) in order to extend the capability of the multi-domain approach.

Bibliography

Brocchini, M., 2013. A reasoned overview on Boussinesq-type models: the interplay between physics, mathematics and numerics. Proceedings of the Royal Society A: Mathematical, Physical and Engineering Sciences 469, 20130496.

Chen, H., Qian, L., Ma, Z., Bai, W., Li, Y., Causon, D., Mingham, C., 2019. Application of an overset mesh based numerical wave tank for modelling realistic free-surface hydrodynamic problems. Ocean Engineering 176, 97–117.

Dentale, F., Reale, F., Di Leo, A., Carratelli, E.P., 2018. A CFD approach to rubble mound breakwater design. International Journal of Naval Architecture and Ocean Engineering 10, 644–650.

Di Lauro, E., Lara, J., Maza, M., Losada, I., Contestabile, P., Vicinanza, D., 2019. Stability analysis of a non-conventional breakwater for wave energy conversion. Coastal Engineering 145, 36–52. doi:10.1016/j.coastaleng.2018.12.008.

Di Paolo, B., Lara, J.L., Barajas, G., Losada, I.J., . Waves and structure interaction using multi-domain couplings for Navier-Stokes solvers in OpenFOAM ®. Part I: Implementation and validation (referred to as Part 1). Coastal Engineering .

El Safti, H., Bonakdar, L., Oumeraci, H., 2014. A hybrid 2D-3D CFD model system for offshore pile groups subject to wave loading. ASME 2014 33rd International Conference on Ocean, Offshore and Arctic Engineering .

Fugazza, M., Natale, L., 1992. Hydraulic design of perforated breakwaters. Journal of Waterway, Port, Coastal, and Ocean Engineering 118, 1–14.

Gotoh, H., Khayyer, A., 2018. On the state-of-the-art of particle methods for coastal and ocean engineering. Coastal Engineering Journal 60, 79–103. doi:10.1080/21664250.2018.1436243.

Higuera, P., Lara, J.L., Losada, I.J., 2013. Simulating coastal engineering processes with OpenFOAM®. Coastal Engineering 71, 119–134.

Hildebrandt, A., Sriram, V., Schlurmann, T., et al., 2013. Simulation of focusing waves and local line forces due to wave impacts on a tripod structure, in: The Twenty-third International Offshore and Polar Engineering Conference, International Society of Offshore and Polar Engineers.

Jacobsen, N.G., van Gent, M.R., Capel, A., Borsboom, M., 2018. Numerical prediction of integrated wave loads on crest walls on top of rubble mound structures. Coastal Engineering 142, 110–124.

Jarlan, G., 1961. A perforated vertical wall breakwater. The Dock and Harbour Authority , 394–398.

Kim, S.H., Yamashiro, M., Yoshida, A., 2010. A simple two-way coupling method of BEM and VOF model for random wave calculations. Coastal Engineering 57, 1018–1028.

Kirby, J.T., 2016. Boussinesq models and their application to coastal processes across a wide range of scales. Journal of Waterway Port Coastal and Ocean Engineering 142.

Lara, J., Ruju, A., Losada, I., 2011. Reynolds Averaged Navier-Stokes modelling of long waves induced by a transient wave group on a beach. Proceedings of the Royal Society A: Mathematical, Physical and Engineering Sciences 467, 1215–1242. doi:10.1098/rspa.2010.0331.

Lara, J.L., Lucio, D., Tomas, A., Di Paolo, B., Losada, I.J., 2019. High-resolution time-dependent probabilistic assessment of the hydraulic performance for historic coastal structures: application to luarca breakwater. Philosophical Transactions of the Royal Society A 377, 20190016.

Larsen, B.E., Fuhrman, D.R., Roenby, J., 2019. Performance of interFoam on the simulation of progressive waves. Coastal Engineering Journal 61, 380–400.

Losada, I.J., Lara, J.L., Guanche, R., Gonzalez-Ondina, J.M., 2008. Numerical analysis of wave overtopping of rubble mound breakwaters. Coastal Engineering 55, 47 – 62.

Martínez-Ferrer, P., Causon, D., Qian, L., Mingham, C., Ma, Z., 2016. A multi-region coupling scheme for compressible and incompressible flow solvers for two-phase flow in a numerical wave tank. Computers & Fluids 125, 116–129.

Martínez-Ferrer, P.J., Qian, L., Ma, Z., Causon, D.M., Mingham, C.G., 2018. An efficient finite-volume method to study the interaction of two-phase fluid flows with elastic structures. Journal of Fluids and Structures 83, 54–71.

Mintgen, F., Manhart, M., 2018. A bi-directional coupling of 2D shallow water and 3D Reynolds-Averaged Navier-Stokes models. Journal of Hydraulic Research 56, 771–785.

Sitanggang, K., Lynett, P., 2010. Multi-scale simulation with a hybrid Boussinesq-RANS hydrodynamic model. International journal for numerical methods in fluids 62, 1013–1046.

Sriram, V., Ma, Q., Schlurmann, T., 2014. A hybrid method for modelling two dimensional non-breaking and breaking waves. Journal of computational physics 272, 429–454.

Tsai, C.P., Ko, C.H., Chen, Y.C., 2018. Investigation on performance of a modified breakwater-integrated OWC wave energy converter. Sustainability 10, 643.

Vandebeek, I., Gruwez, V., Altomare, C., Suzuki, T., Vanneste, D., De Roo, S., Toorman, E., Troch, P., 2018. Towards an efficient and highly accurate coupled numerical modelling approach for wave interactions with a dike on a very shallow foreshore, in: Coastlab 2018, pp. 1–10.

Verbrugghe, T., Domínguez, J.M., Crespo, A.J., Altomare, C., Stratigaki, V., Troch, P., Kortenhaus, A., 2018. Coupling methodology for smoothed particle hydrodynamics modelling of non-linear wave-structure interactions. Coastal Engineering 138, 184–198.

Wang, D.x., Dong, S., Sun, J.w., 2019. Numerical modeling of the interactions between waves and a Jarlan-type caisson breakwater using OpenFOAM. Ocean Engineering 188, 106230.

Zijlema, M., Stelling, G., Smit, P., 2011. SWASH: An operational public domain code for simulating wave fields and rapidly varied flows in coastal waters. Coastal Engineering 58, 992–1012.